Supplementary Information for

Helically Twisted Nanoribbons via Stereospecific Annulative π-Extension Reaction Employing [7]Helicene as a Molecular Wrench

Asim Swain[1], Krzysztof Radacki,[2] Holger Braunschweig,[2] and Prince Ravat[1,*]

[1]Julius-Maximilians-Universität Würzburg, Institut für Organische Chemie, Am Hubland, 97074 Würzburg, Germany

[2]Julius-Maximilians-Universität Würzburg, Institut für Anorganische Chemie, Am Hubland, 97074 Würzburg, Germany

*Email: princekumar.ravat@uni-wuerzburg.de

Table of Contents

S1. Experimental Details

General Information. All chemicals and solvents were purchased from commercial sources and were used without further purification unless stated otherwise. 3,3'-Dibromo-4,4'-biphenanthrene[1], 2,7-di-tert-butylpyrene[2], 2,2'-(2,7-di-tert-butylpyrene-4,9-diyl)bis(4,4,5,5-tetramethyl-1,3,2-dioxaborolane) and 2-(2,7-di-*tert*-butylpyren-4-yl)-4,4,5,5-tetramethyl-1,3,2-dioxaborolane[3], 2,2',6,6'-tetrabromo-4,4'-di-tert-butyl-1,1'-biphenyl[4] and [Pd(CH$_3$CN)$_4$](SbF$_6$)$_2$[5] were synthesized according to literature known protocols and purity was confirmed by ^{1}H NMR. The reactions and experiments sensitive to dioxygen were performed using Schlenk techniques and with nitrogen-saturated solvents. Prior to use all the glassware and NMR tubes were dried in oven at 80 °C for 12 h.

Chromatography. Open-column chromatography and thin-layer chromatography (TLC) were performed on silica gel (Merck silica gel 100-200 mesh). Chiral stationary phase HPLC separations were performed by SHIMADZU 223.

NMR Spectroscopy. The NMR measurements were performed at 298 K on NMR spectrometers operating at 400 MHz proton and 101 MHz ^{13}C frequencies. Standard pulse sequences were used, and the data was processed using 2-fold zero-filling in the indirect dimension for all 2D experiments. Chemical shifts (δ) are reported in parts per million (ppm) relative to the solvent residual peak (^{1}H and ^{13}C NMR, respectively): CDCl$_3$ ($\delta = 7.26$ and 77.2 ppm), CD$_2$Cl$_2$ ($\delta = 5.32$ and 53.84 ppm) and J values are given in Hz. Structural assignments for all synthesized compounds were made using additional information obtained from *g*COSY, *g*NOESY, *g*HSQC, and *g*HMBC experiments.

High resolution mass spectrometry (HRMS). The matrix assisted laser desorption ionization-time of flight (MALDI-TOF) - HRMS were measured on Bruker ultrafleXtreme. *Trans*-2-[3-(4-*tert*-butylphenyl)-2-methyl-2-propenylidene]malononitrile (DCTB) dissolved in chloroform (30 mg/mL) was used as supporting matrix, while Caesium iodide dissolved in acetonitrile (40 mg/mL) used as reference in the MALDI-TOF–HRMS measurement. The calculated mass was exported from mMass software.[6]

Melting point. Melting points were measured using an OptiMelt Automated Melting Point System.

UV−Vis and Fluorescence spectroscopy. UV−Vis spectra were measured on JASCO V-670 spectrometer, while emissiosn spectra were measured Edinburgh FLS 980 photoluminescence

spectrometer in DCM (OD = 0.05). The fluorescence lifetimes were measured in DCM (OD = 0.05) using a 418.6 nm pulsed laser diode with a pulse frequency of 1/50 ns. The fluorescence quantum yields were measured in DCM in three different concentration (OD = 0.2 – 0.5) using same spectrometer with a 450 W xenon arc lamp as a light source and a calibrated integrating sphere.

CPL and CD spectroscopy. CPL and CD spectra were recorded with a customized JASCO CPL-300/J-1500 hybrid spectrometer.

Single-Crystal X-ray Crystallography. The crystal data were collected on a RIGAKU XTALAB SYNERGY – R diffractometer with a HPA area detector and multi-layer mirror monochromated $Cu_{K\alpha}$ radiation. The structure was solved using intrinsic phasing method[7], refined with the SHEL XL program[8] and expanded using Fourier techniques. All non-hydrogen atoms were refined anisotropically. Hydrogen atoms were included in structure factors calculations. All hydrogen atoms were assigned to idealized geometric positions.

Quantum chemical calculations. DFT calculations were performed using Gaussian 16 suite.[9] Geometries were optimized using ωB97XD functional and 6-31G(d,p) basis set in the gas phase. Frequency analysis was performed to verify the stationary state geometry. In all cases no imaginary frequency was found. TD-DFT calculations were performed on ωB97XD/6-31G(d,p) optimized geometries at the B3LYP/6-31g(d,p) level. The effect of the solvent was accounted for using PCM (with dichloromethane as the solvent). SpecDis[10] and Avogadro[11] software were used to analyze the TD-DFT calculated spectra, and to generate graphical images of frontier molecular orbitals (FMOs), respectively.

S2. Reaction Procedures and Characterizations

Synthesis of (*P*)-Dimethylsila[7]helicene.
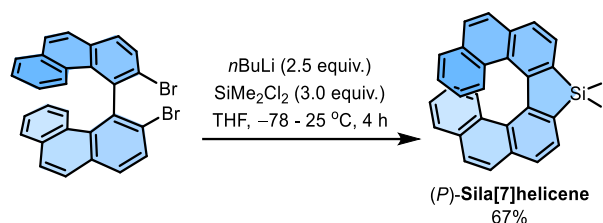
(*P*)-**Sila[7]helicene**
67%

(*P*)-**Dimethylsila[7]helicene** was synthesized with a modified literature procedure.[12] In a Schlenk tube 3,3'-Dibromo-4,4'-biphenanthrene (450 mg, 0.88 mmol) was dissolved in 25 mL of dry THF (tetrahydrofuran). The reaction mixture was degassed for 20 minutes at –78 °C. 1.2 mL (2.20 mmol) of *n*BuLi was added dropwise and stirred for 30 minutes. The TLC confirmed the completion of lithiation process, Me$_2$SiCl$_2$ (0.32 mL, 2.64 mmol) was added to the reaction mixture dropwise. The reaction mixture was slowly warmed to room temperature and stirred for 4 h. The reaction was quenched with water, and the organic layer was extracted with ethyl acetate and dried over sodium sulphate. The combined organic layer was evaporated under reduced pressure. The crude product was then purified with silica gel column chromatography using petrolether to yield 241 mg (67%) of sila[7]helicene as yellow crystalline solid.

Characterization of (*P*)-Dimethylsila[7]helicene.

HRMS (MALDI-TOF) m / z: [M] Calcd for [C$_{30}$H$_{22}$Si] 410.1491; Found 410.1508

^{1}H NMR (400 MHz, CDCl$_3$, 25 °C): δ [ppm] = 7.84 (d, *J* = 7.3 Hz, 2H), 7.78 (d, *J* = 7.4 Hz, 2H), 7.66 (d, *J* = 8.7 Hz, 2H), 7.51 (d, *J* = 8.7 Hz, 2H), 7.36 (d, *J* = 9.4 Hz, 2H), 7.32 (d, *J* = 9.2 Hz, 2H), 6.97 – 6.91 (m, 2H), 6.37 – 6.33 (m, 2H), 0.60 (s, 6H).

^{13}C NMR (101 MHz, CDCl$_3$, 25 °C): δ [ppm] = 147.73, 139.58, 134.25, 132.14, 130.33, 128.96, 128.88, 127.72, 127.25, 126.72, 126.53, 126.05, 125.05, 122.99, –2.60.

Synthesis of 3Py.

3Py
78%
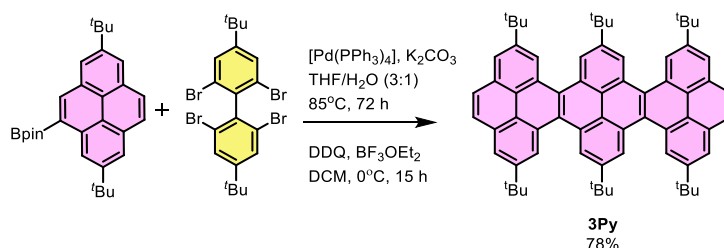
3Py was synthesized with a modified literature procedure.[13] In a Schlenk tube 2-(2,7-di-tert-butylpyren-4-yl)-4,4,5,5-tetramethyl-1,3,2-dioxaborolane (30 mg, 0.068mmol) and 2,2',6,6'-tetrabromo-4,4'-di-tert-butyl-1,1'-biphenyl (20 mg, 0.034 mmol) were dissolved in 3 mL dry

THF and potassium carbonate (14.1 mg, 0.102 mmol) was dissolved in water (1 mL) and both solutions were degassed for 10 min separately and mixed together. To this mixture tetrakis(triphenylphosphine)palladium(0) [Pd(PPh$_3$)$_4$] (4.0 mg, 10.0 mol %) was added under nitrogen flow and degassed again for 10 min. The reaction flask was then sealed with Teflon tape and heated at 85 °C for 72 h in an oil bath. The organic layer was extracted with ethyl acetate and dried over anhydrous sodium sulfate. The solvent was evaporated under reduced pressure using a rotary evaporator and crude product was passed through small plug of silica column using 1−2% ethyl acetate in petroleum ether to remove inorganic impurities. The crude product was then dissolved in dry DCM (3 mL) and subjected to Scholl-type cyclodehydrogenation in the presence of DDQ (10 mg, 0.044 mmol) and BF$_3$OEt$_2$ (0.15 mL, 1.21 μmol) at 0 °C and warmed up to room temperature overnight (15 h). The reaction was quenched with sodium bicarbonate and the organic layer was extracted with DCM. The collected organic phase was dried over anhydrous sodium sulphate. The solvent was evaporated under reduced pressure using a rotary evaporator and crude product was passed through silica gel column using 10% ethyl acetate in petroleum ether to isolate **3Py** in 78% yield (23.8 mg) as yellow solid over two steps.

Characterization of 3Py.

HRMS (MALDI-TOF) m / z: [M] Calcd for [C$_{68}$H$_{70}$] 886.5477; Found 886.5469

^{1}H NMR (400 MHz, CDCl$_3$, 25 °C): δ [ppm] = 9.26 – 9.28 (m, 8H), 8.30 (d, J = 1.5 Hz, 4H), 8.15 (s, 4H), 1.63 (s, 54H).

^{13}C NMR (101 MHz, CDCl$_3$, 25 °C): δ [ppm] = 148.48, 148.28, 131.19, 129.51, 129.12, 128.96, 127.68, 123.38, 123.24, 123.00, 122.95, 122.37, 36.02, 35.67, 32.41, 32.28.

Synthesis of (P, P)-1 by one pot Suzuki coupling – C-H activation.

In a Schlenk tube (S)-3,3'-dibromo-4,4'-biphenanthrene (70.0 mg, 0.13 mmol) and 2,2'-(2,7-di-tert-butylpyrene-4,9-diyl)bis(4,4,5,5-tetramethyl-1,3,2-dioxaborolane) (36.5 mg, 0.065 mmol) were dissolved in 3 mL dry THF and potassium carbonate (44.5 mg, 0.32 mmol) was dissolved in 1 mL water and both solutions were degassed for 10 min separately and mixed together. To

this mixture [Pd(PPh$_3$)$_4$] (7.5 mg, 10.0 mol %) was added under nitrogen flow and degassed again for 10 min. The reaction flask was then sealed with Teflon tape and heated at 85 °C for 72 h in an oil bath. The reaction was quenched by adding water and extracted with ethyl acetate. The collected organic phase was dried over anhydrous sodium sulfate. The solvent was evaporated under reduced pressure using a rotary evaporator and crude product was passed through silica column using 1−2% ethyl acetate in petroleum ether to isolate (P, P)-**1** in 35% (24.3 mg) yield.

Characterization of (P, P)-1.

Melting point: 196–198 °C

HRMS (MALDI-TOF) m / z: [M] Calcd for [C$_{80}$H$_{54}$] 1014.4226; Found 1014.4251

^{1}H NMR (400 MHz, CDCl$_3$, 25 °C): δ [ppm] = 9.39 (s, 4H), 9.12 (d, J = 8.6 Hz, 4H), 8.20 (d, J = 8.7 Hz, 4H), 7.80 (d, J = 8.5 Hz, 4H), 7.55 (d, J = 8.2 Hz, 4H), 7.43 (d, J = 8.9 Hz, 4H), 7.39 (d, J = 8.0 Hz, 4H), 7.04 – 7.00 (m, 4H), 6.64 – 6.59 (m, 4H), 1.89 (s, 18H).

^{13}C NMR (101 MHz, CDCl$_3$, 25 °C): δ [ppm] = 148.47, 132.26, 131.09, 129.64, 129.53, 128.90, 128.56, 128.23, 128.19, 127.78, 126.96, 125.90, 125.59, 125.36 (overlapped with two signals), 125.22, 124.05, 123.87, 123.78, 36.30, 32.38.

Synthesis of (P, M)-1. The Suzuki coupling−C-H activation was performed with 2,2'-(2,7-di-tert-butylpyrene-4,9-diyl)bis(4,4,5,5-tetramethyl-1,3,2-dioxaborolane) and rac-3,3'-dibromo-4,4'-biphenanthrene. The HPLC chromatogram of isolated diastereomeric mixture of **1** showed formations of chiral (P*, P*)-**1** to meso (P, M)-**1** in a 3.8:1 ratio. The (P, M)-**1** ^{1}H NMR is similar to that of (P, P)-**1** with a mere shift of 0.02 – 0.05 ppm in chloroform at room temperature.

Synthesis of (P, P)-1 by APEX reaction.

(P, P)-**1** 7%   (P)-**VII** 36%
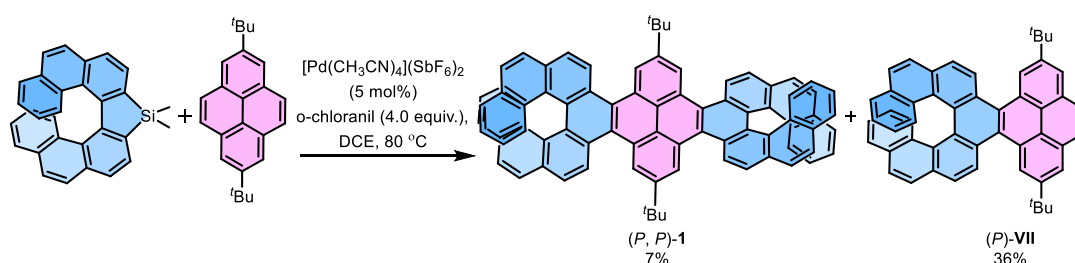
(P)-Dimethylsila[7]helicene (69 mg, 0.167 mmol, 3.5 equiv.), 2,7-di-tert-butylpyrene (15 mg, 0.048 mmol), [Pd(CH$_3$CN)$_4$](SbF$_6$)$_2$ (1.8 mg, 5.0 mol%) and o-chloranil (47 mg, 0.191 mmol) were dissolved in dry dichloroethane (DCE) (2 mL) and degassed for 20 minutes. The reaction mixture was heated at 80 °C for 15 h in an oil bath. The reaction mixture was cooled down to

room temperature and DCE was evaporated under reduced pressure using rotary evaporator. The crude mixture was passed through silica column with petroleum ether – 2% ethyl acetate in petroleum ether to recover 7 mg (0.022 mmol) of 2,7-di-tert-butylpyrene along with (*P, P*)-**1** in 7% (1.9 mg, 0.002 mmol) and (*P*)-**VII** in 36% (6.2 mg, 0.358 mmol) conversion. (The isolated conversion efficiency is calculated considering the amount of 2,7-di-*tert*-butylpyrene reacted.) The isolated (*P, P*)-**1** was passed through chiral stationary phase HPLC to show single peak confirming the stereoselectivity of the reaction.

Synthesis of (*P*, *P*)-2, (*P*)-3, and (*P*)-3_Cl by APEX reaction.
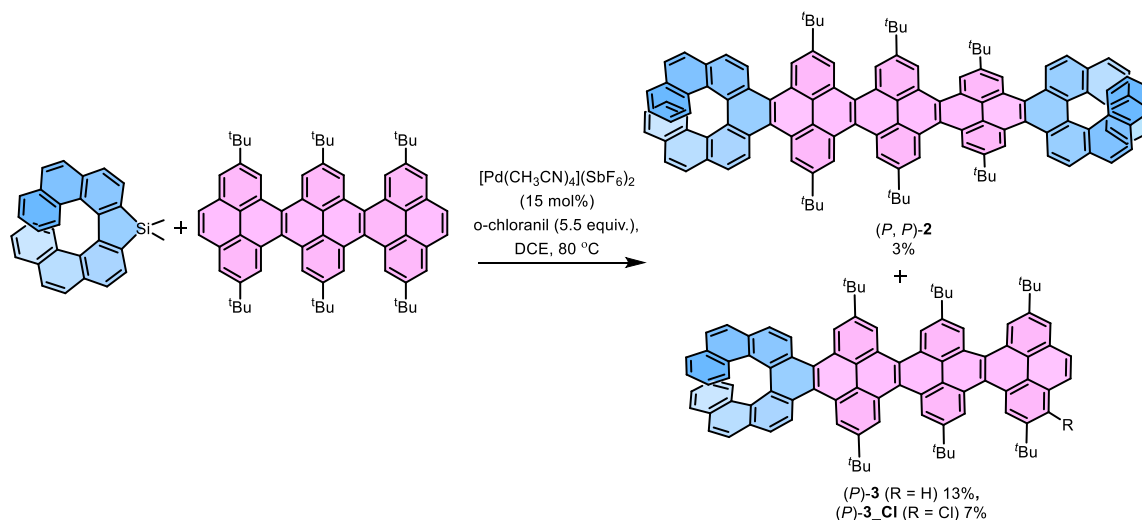
(*P*)-Dimethyl**s**ila[7]helicene (56 mg, 0.135 mmol), **3Py** (20 mg, 0.022 mmol), [Pd(CH$_3$CN)$_4$](SbF$_6$)$_2$ (2.5 mg, 15.0 mol%) and o-chloranil (30.5 mg, 0.124 mmol) were dissolved in 2 mL dry DCE and degassed for 20 minutes. The reaction mixture was heated at 80 °C for 15 h in an oil bath. The reaction mixture was cooled down to room temperature and DCE was evaporated under reduced pressure using rotary evaporator. The reaction was repeated four times and the combined crude mixture was passed through silica column with petroleum ether – 2% ethyl acetate in petroleum ether to recover 38 mg (0.043 mmol) of **3Py** along with (*P*)-**3** in 13% (7.6 mg, 0.006 mmol) and (*P*)-**3_Cl** in 7% (4.3 mg, 0.003 mmol) conversion. Further ethyl acetate concentration in the eluent mixture was increased gradually by 1 ml in each addition of 1000 ml of solvent to isolate (*P, P*)-**2** in 3% (2.1 mg, 0.001 mmol) conversion. (The isolated conversion efficiencies are calculated considering the amount of **3Py** reacted.)

Characterization of (*P*, *P*)-2.

HRMS (MALDI-TOF) m / z: [M] Calcd for [C$_{124}$H$_{98}$] 1587.7702; Found 1587.7721

¹H NMR (400 MHz, CD₂Cl₂, 25 °C): δ [ppm] = δ 9.44 (d, J = 1.5 Hz, 4H), 9.40 – 9.35 (m, 8H), 9.20 (d, J = 8.5 Hz, 4H), 8.27 (d, J = 8.6 Hz, 4H), 7.86 (d, J = 8.6 Hz, 4H), 7.59 (d, J = 9.0 Hz, 4H), 7.45 (d, J = 9.4 Hz, 4H), 7.42 (d, J = 9.5 Hz, 4H), 7.07 – 7.03 (m, 4H), 6.64 – 6.60 (m, 4H), 1.80 (s, 36H), 1.71 (s, 18H).

¹³C NMR (101 MHz, CD₂Cl₂, 25 °C): δ [ppm] = 149.05, 148.95, 132.53, 131.40, 130.22, 129.80, 129.76, 129.69, 129.22, 129.04, 128.87, 128.57, 128.37, 127.94, 127.18, 126.19, 125.76, 125.57, 125.46, 125.44, 124.72, 124.05, 123.69, 123.27, 122.93, 36.33, 36.29, 32.44, 32.31.

Characterization of (*P*)-3.

HRMS (MALDI-TOF) m / z: [M] Calcd for [C₉₆H₈₄] 1237.6563; Found 1237.6581

¹H NMR (400 MHz, CDCl₃, 25 °C): δ [ppm] = 9.40 (d, J = 1.3 Hz,, 2H), 9.35 – 9.28 (m, 8H), 9.16 (d, J = 8.5 Hz, 2H), 8.31 (d, J = 1.7 Hz, 2H), 8.21 (d, J = 8.7 Hz, 2H), 8.16 (s, 2H), 7.81 (d, J = 8.6 Hz, 2H), 7.56 (d, J = 8.4 Hz, 2H), 7.45 (d, J = 8.5 Hz, 2H), 7.39 (d, J = 7.4 Hz, 2H), 7.05 – 7.01 (m, 2H), 6.64 – 6.60 (m, 2H), 1.78 (s, 18H), 1.66 (s, 18H), 1.64 (s, 18H).

¹³C NMR (101 MHz, CDCl₃, 25 °C): δ [ppm] = 148.52, 148.38, 148.35, 132.26, 131.22, 131.08, 129.66, 129.59, 129.53, 129.21, 129.07, 129.03, 129.00, 128.92, 128.66, 128.24, 128.19, 127.76, 127.71, 126.97, 125.91, 125.64, 125.34, 125.29, 125.24, 124.40, 123.78, 123.59, 123.42, 123.27, 123.11, 123.04, 122.98, 122.80, 122.41, 122.21, 36.16, 36.06, 35.70, 32.43, 32.38, 32.30.

Characterization of (*P*)-3_Cl.

HRMS (MALDI-TOF) m / z: [M] Calcd for [C₉₆H₈₃Cl] 1271.6183; Found 1271.6189

¹H NMR (400 MHz, CDCl₃, 25 °C): δ [ppm] = 9.41 (d, J = 1.7 Hz, 2H), 9.35 – 9.28 (m, 7H), 9.19 (d, J = 1.6 Hz, 1H), 9.16 (d, J = 8.5 Hz, 2H), 8.78 (d, J = 9.4 Hz, 1H), 8.35 (d, J = 1.7 Hz, 1H), 8.27 (d, J = 9.5 Hz, 1H), 8.21 (d, J = 8.6 Hz, 2H), 7.81 (d, J = 8.6 Hz, 2H), 7.56 (d, J = 8.5 Hz, 2H), 7.47 – 7.42 (m, 2H), 7.39 (d, J = 8.0, 2H), 7.05 – 7.01 (m, 2H), 6.64 – 6.60 (m, 2H), 1.82 – 1.76 (m, 27H), 1.68 – 1.64 (m, 27H).

¹³C NMR (101 MHz, CDCl₃, 25 °C): δ [ppm] = 149.37, 148.56, 148.52, 148.37, 148.34, 143.60, 132.26, 131.08, 130.92, 129.87, 129.65, 129.57, 129.52, 129.50, 129.42, 129.37, 129.33, 129.20, 129.11, 129.09, 129.03, 128.92, 128.87, 128.63, 128.26, 128.20, 127.78, 127.50, 126.97, 125.91, 125.61, 125.35, 125.30, 125.23, 125.09, 124.70, 124.47, 123.97, 123.86, 123.78, 123.61, 123.41, 123.39, 123.20, 123.09, 123.00, 122.76, 122.72, 122.68, 122.58, 122.57, 122.51, 37.63, 36.16, 36.08, 35.74, 32.43, 32.41, 32.38, 32.30, 32.25, 30.87, 29.90.

S3. Chiral stationary phase HPLC
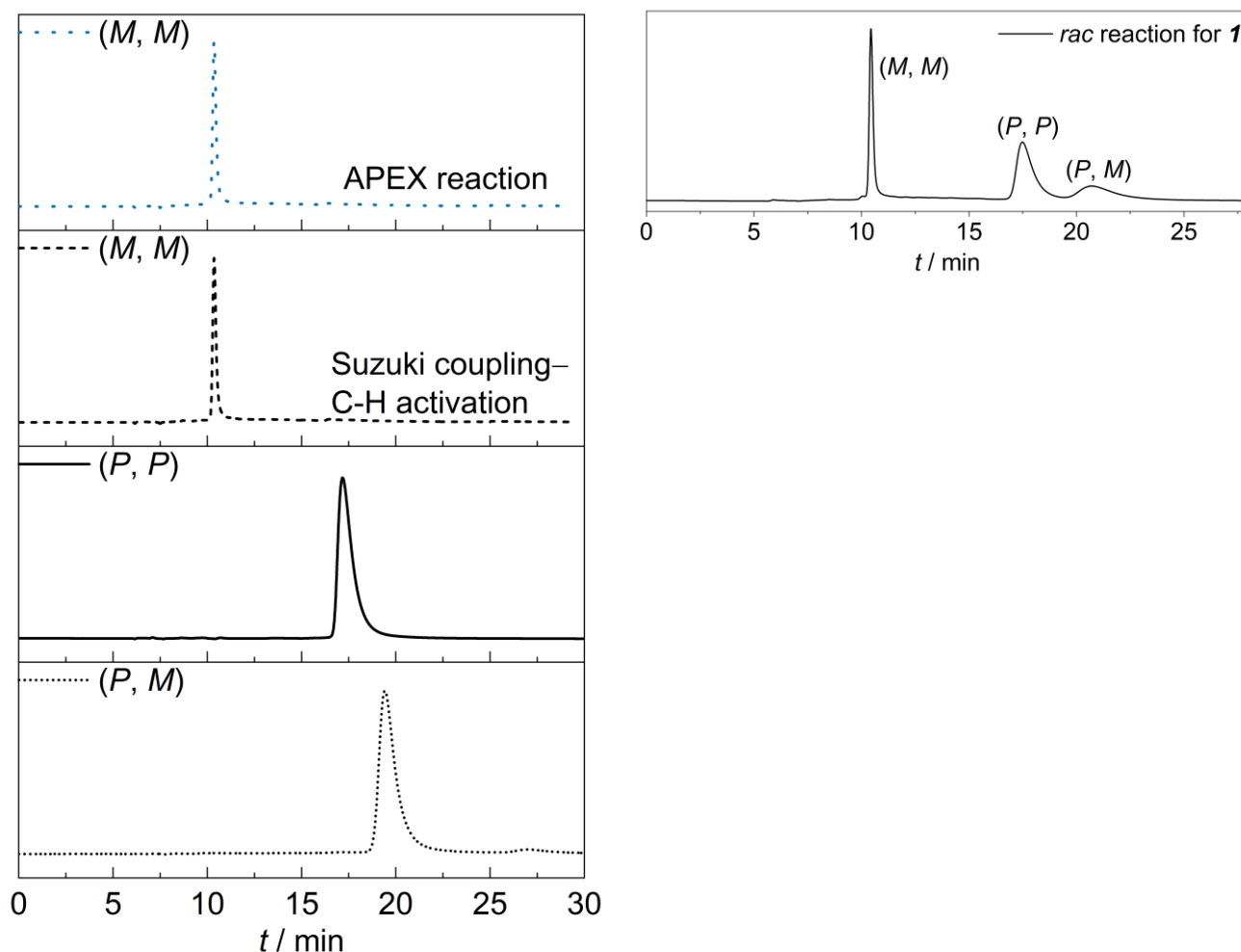
Figure S1. HPLC chromatogram of **1** using chiral stationary phase column. (The chromatogram detector was set at 354 nm with a bandwidth of 4 nm.)

Table S1. Overview of parameters for HPLC separation of enantiomers of **1**.

Compound	Eluent n-hexane/iPrOH	First fraction	Second fraction	Third fraction	α^b	Rs^c	er
1	97:3	*MM*	*PP*	*PM*	1.63	1.79	99:1

[a]Phenomenex Lux i-Amylose-3 5 μm (250 x 4.6 mm). Sample injection: 30 μL of a ~1 mg/mL solution in hexane/iPrOH. Separation conditions: Eluent, flow rate: 0.5 mL/min, 25 °C. [b]Selectivity parameter: $\alpha = t_{R2}/t_{R1}$, where t_{R1}, and t_{R2} are elution times for first and second fraction, respectively. [c]Resolution parameter: $R_S = 2(t_{R2} - t_{R1})/(w_1 + w_2)$, where w_1 and w_2 are peak widths for first and second fraction, respectively. Note α and Rs was calculated only for *PP* and *MM*.

S4. Determination and analysis of activation parameters for diastereomerization of 1.

(a)

(b)
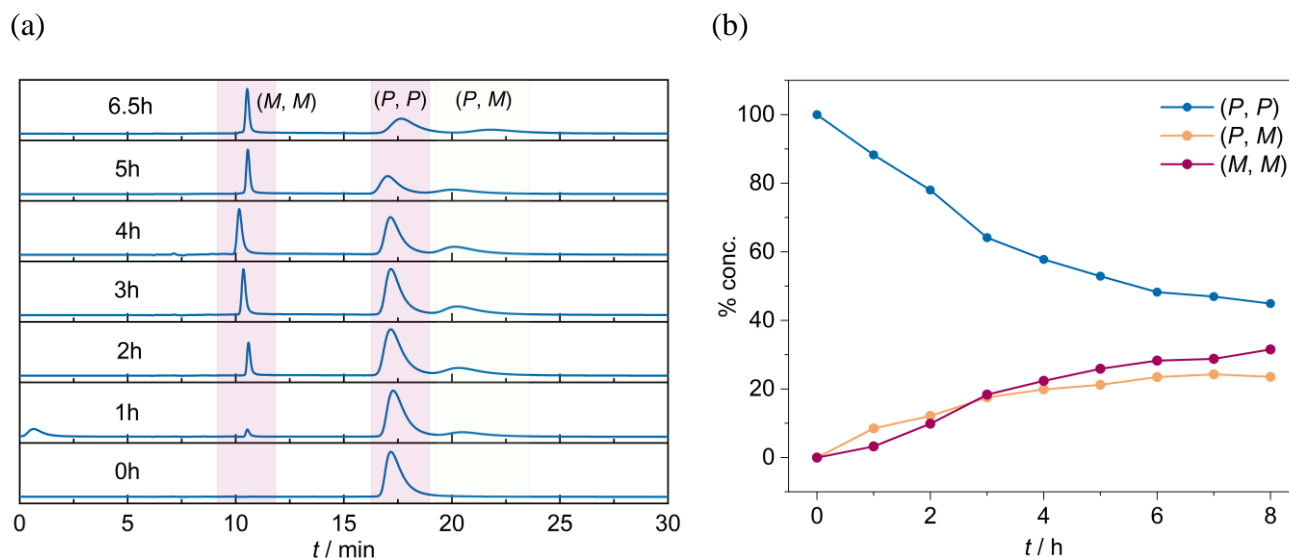
Figure S2. HPLC chromatogram of (P, P)-**1** upon heating at 173 °C over time using chiral stationary phase column. (The HPLC chromatogram detector was set at 354 nm with a bandwidth of 4 nm.)

The Gibbs activation energies ($\Delta G^{\ddagger}$ (T)) for diastereomerization of **1** calculated by following the decay of the diastereomeric excess (de) of (P, P)-**1** dissolved in diethylene glycol dibutyl ether (1-(2-(2-butoxyethoxy)ethoxy)butane) at 423, 433, 443, 453 K over time (t) by HPLC on a chiral stationary phase. To estimate the $\Delta G^{\ddagger}$ (T) value, the $\ln(de_t/de_0)$ values were plotted against t and the data set was linearly fitted (Figure **S3**). Following the equation

$$ln\left(\frac{de_t}{de_0}\right) = -k_d t$$

the k_d (diastereomerization rate constant) values were obtained.

The enthalpy (ΔH) and entropy (ΔS) values were obtained using the following equation

$$ln\left(\frac{k_d}{T}\right) = \left(ln\left(\frac{\kappa k_B T}{h}\right) + \frac{\Delta S}{R}\right) - \left(\frac{\Delta H}{R}\right)\left(\frac{1}{T}\right)$$

where, R is the gas constant (R = 8.31446 J K^{-1}), h is the Planck constant (h = 6.62607 × 10^{-34} J s), k_B is the Boltzmann constant (k_B = 1.38064852 × 10^{-23} J K^{-1}), and κ is the transmission coefficient (κ = 0.5 or 1). The transmission coefficient κ = 0.5 was used because the diastereomerization process is defined as a reversible first order reaction.

(a)

(b)

(c)

(d)
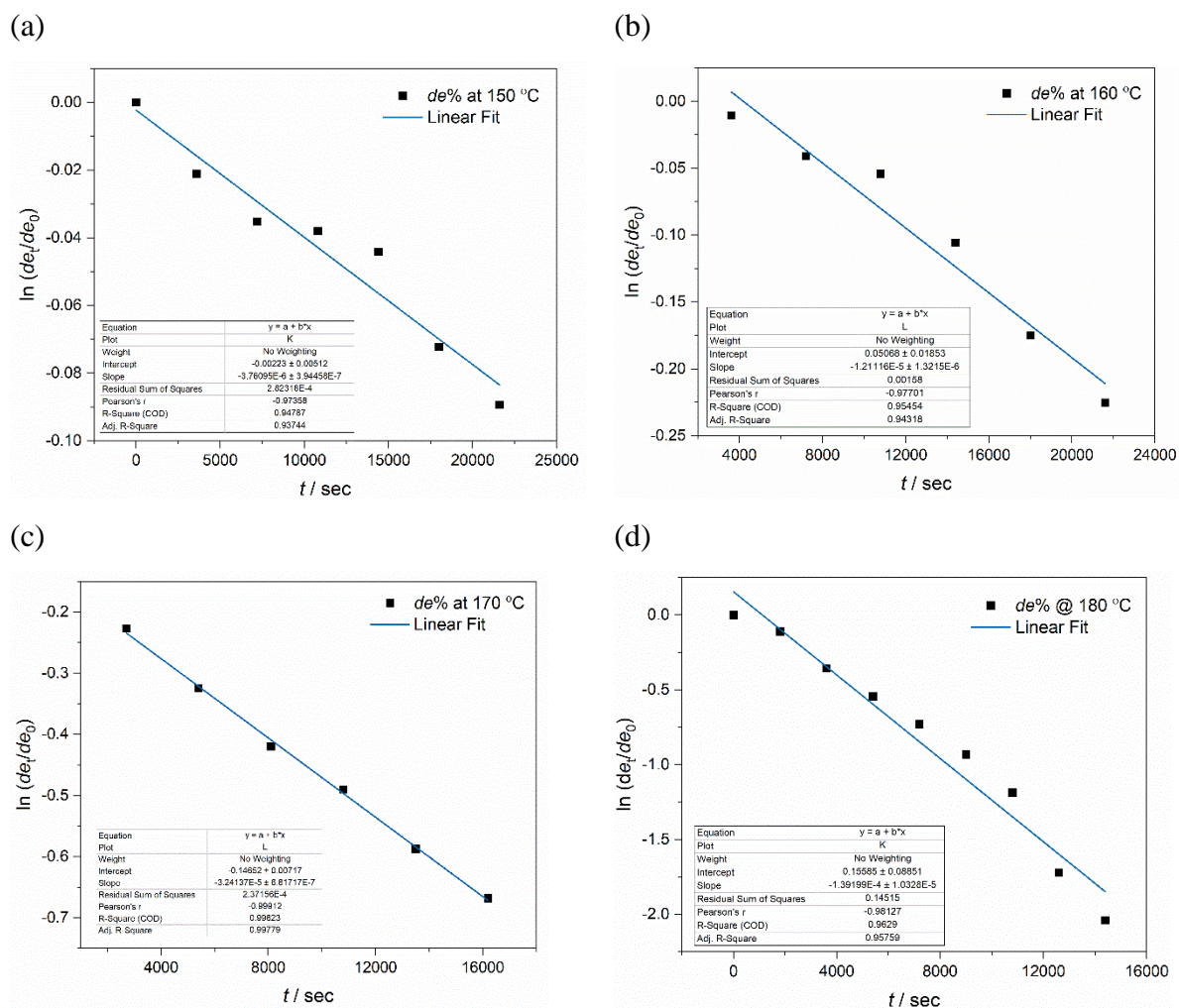
Figure S3a. Plot of ln(de_t/de_0) against t for **1** fitted linearly to obtain the k_d value.

ΔH = 44.1 kcal mol^{-1}
ΔS = 21.4 cal K^{-1} mol^{-1}
$\Delta G^{\ddagger}$ (298 K) = 37.7 kcal mol^{-1}

T = 423 K – 453 K
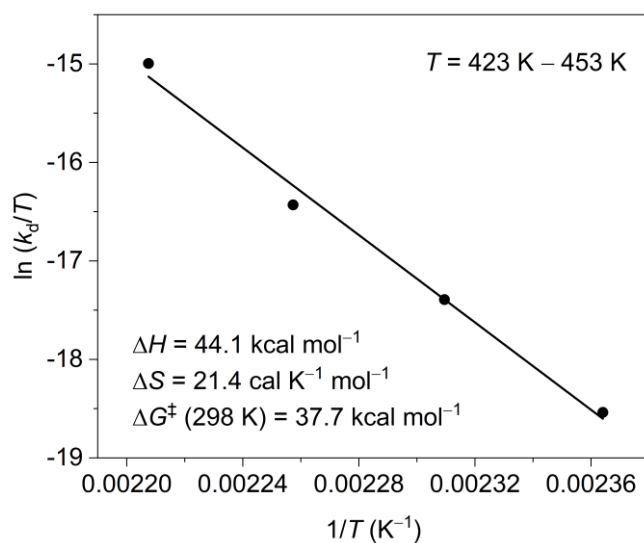
Figure S3b. Plot of ln(k_d/T) against $1/T$ for (P, P)-**1** fitted linearly to obtain the ΔH and ΔS values.

S5. Photophysical Studies

a. Absorption and Emission Spectroscopy

(a)   (b)

(c)   (d)
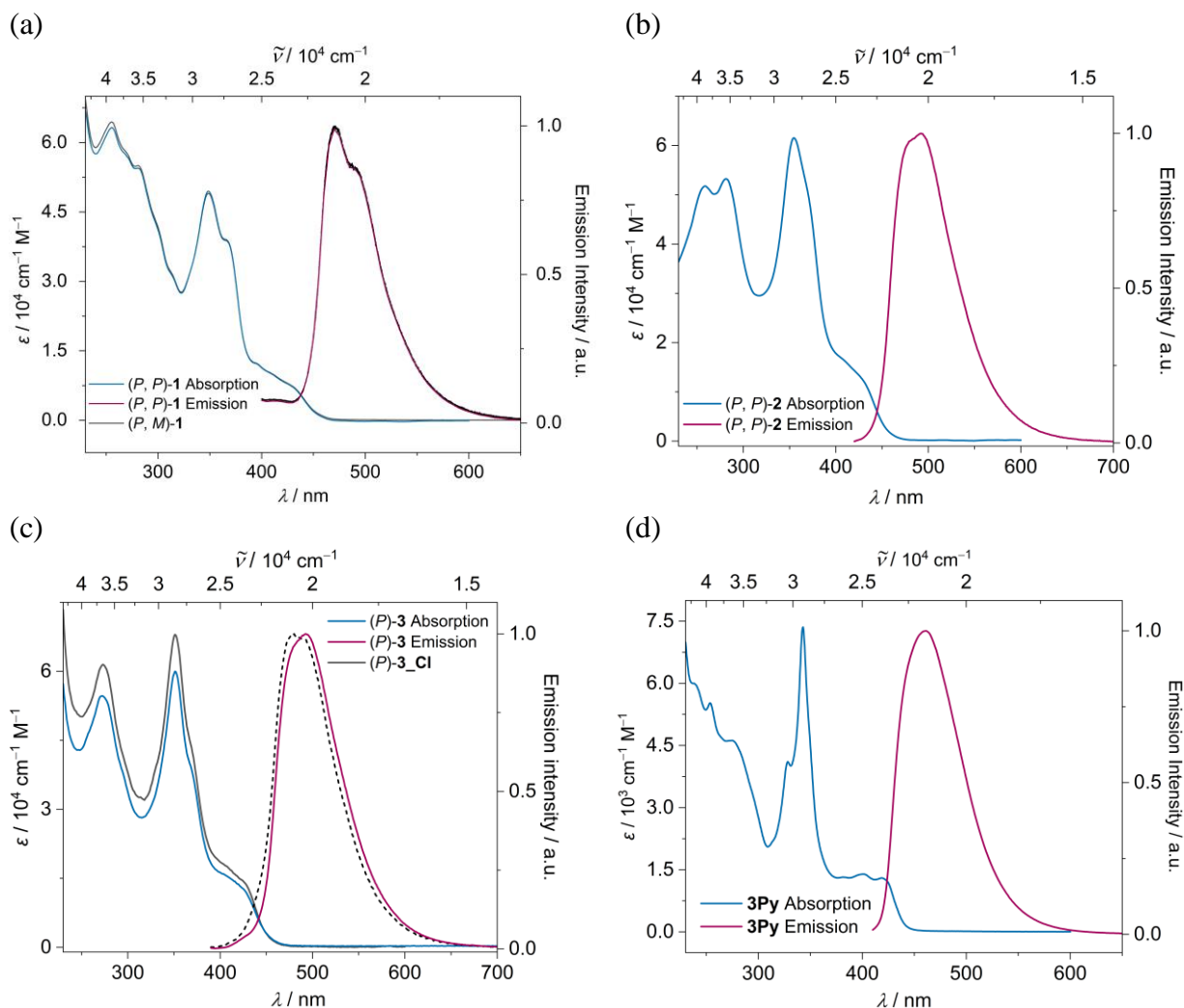
Figure S4. UV–Vis absorption (blue) and emission (red) spectra of (a) (*P*, *P*)-**1** and (*P*, *M*)-**1**, (b) (*P*, *P*)-**2**, (c) (*P*)-**3** and (*P*)-**3_Cl**, (d) **3Py** in dichloromethane (c~10^{-5} M).

Table S2. Summary of (chir)optical parameters.

Compound	λ_{maxabs} (nm)/ ε (cm⁻¹ M⁻¹)	$\lambda_{max\ em}$ (nm)	E_g / eV[a]	Φ_{FL}	τ_{FL} / ns	k_{FL} / 10^8 s⁻¹	k_{NR} / 10^8 s⁻¹	g_{abs}[d] / 10^{-3}	g_{lum} / 10^{-3}
(*P*, *P*)-**1**	431 (7325)	473	2.83	0.05	5.55[b]	0.09[c]	1.72[c]	2.64 − 1.17	0.63
(*P*, *M*)-**1**	430 (7167)	472	2.83	0.04	5.62[b]	0.07[c]	1.71[c]	−	−
(*P*, *P*)-**2**	425 (13393)	492	2.79	0.15	5.07	0.29	1.68	4.05 − 1.92	1.54
(*P*)-**3**	426 (12533)	493	2.80	0.19	5.13	0.37	1.58	2.43 − 1.16	0.54
(*P*)-**3_Cl**	428 (13691)	480	2.84	0.22	5.09[b]	0.43	1.53[c]	3.46 − 0.87	0.83
3Py	420(1293)	461	2.92	0.21	3.92[b]	0.54	2.01[c]	−	−

[a]Estimated from a crossing of absorption and fluorescence spectra [b]$\tau_{avg}^{[14]} = (\alpha_1 \tau_1^2 + \alpha_2 \tau_2^2)/(\alpha_1 \tau_{1+} \alpha_2 \tau_2)$ [c]Calculated for τ_{avg} [d]Wavelength range $230 - 450$ nm

b. Time resolved fluorescence decay.
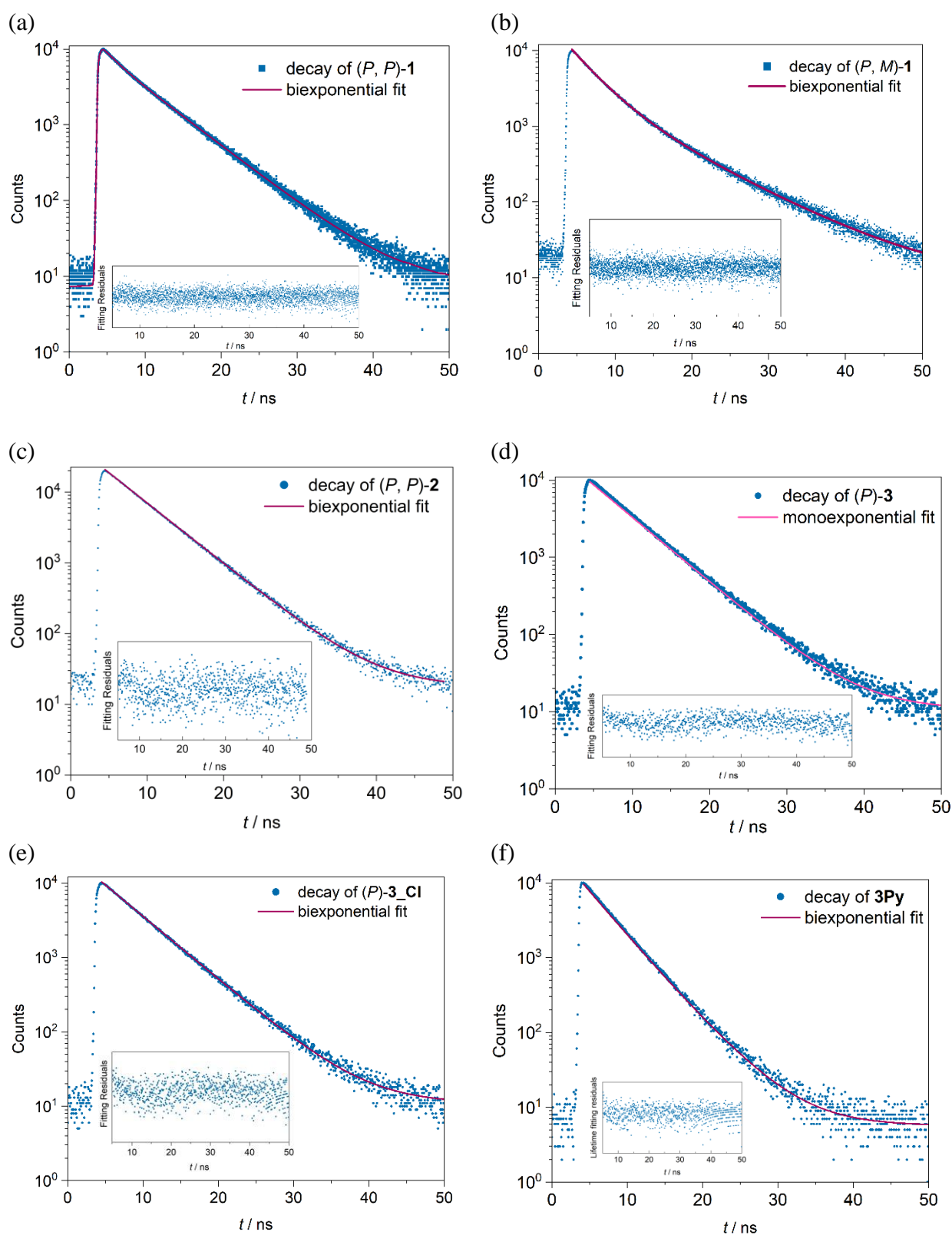
Figure S5. Time resolved fluorescence decay (excited at 24154 cm^{-1}) of (a) (*P*, *P*)-**1,** (b) (*P*, *M*)-**1**, (c) (*P*, *P*)-**2**, (d) (*P*)-**3**, (e) (*P*)-**3_Cl** (f) **3Py** in dichloromethane (c~10^{-5} M). Inset- fitting residuals.

c. ECD and CPL spectroscopy

(a)

(b)

(c)

(d)

(e)

(f)
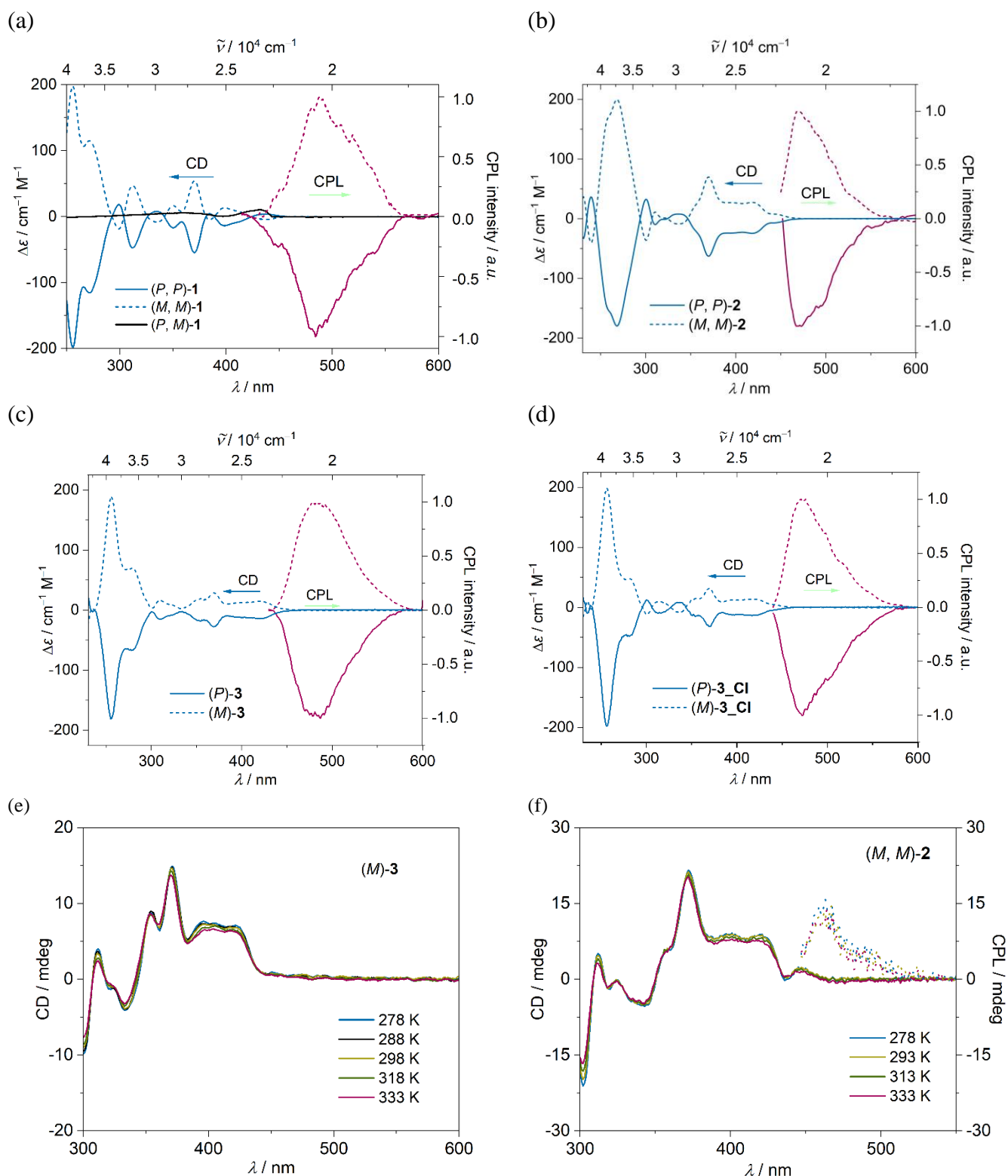
Figure S6. ECD (blue) and CPL (red) spectra of (a) **1**, (b) **2**, (c) **3** and (d) **3_Cl** in dichloromethane and variable temperature ECD (solid) and CPL (dotted) spectra of (e) (*M*)-**3**, (f) (*M*, *M*)-**2** in toluene (c∼10^{-5} M).

d. Absorption and luminescence dissymmetry factors.

(a)

(b)

(c)

(d)
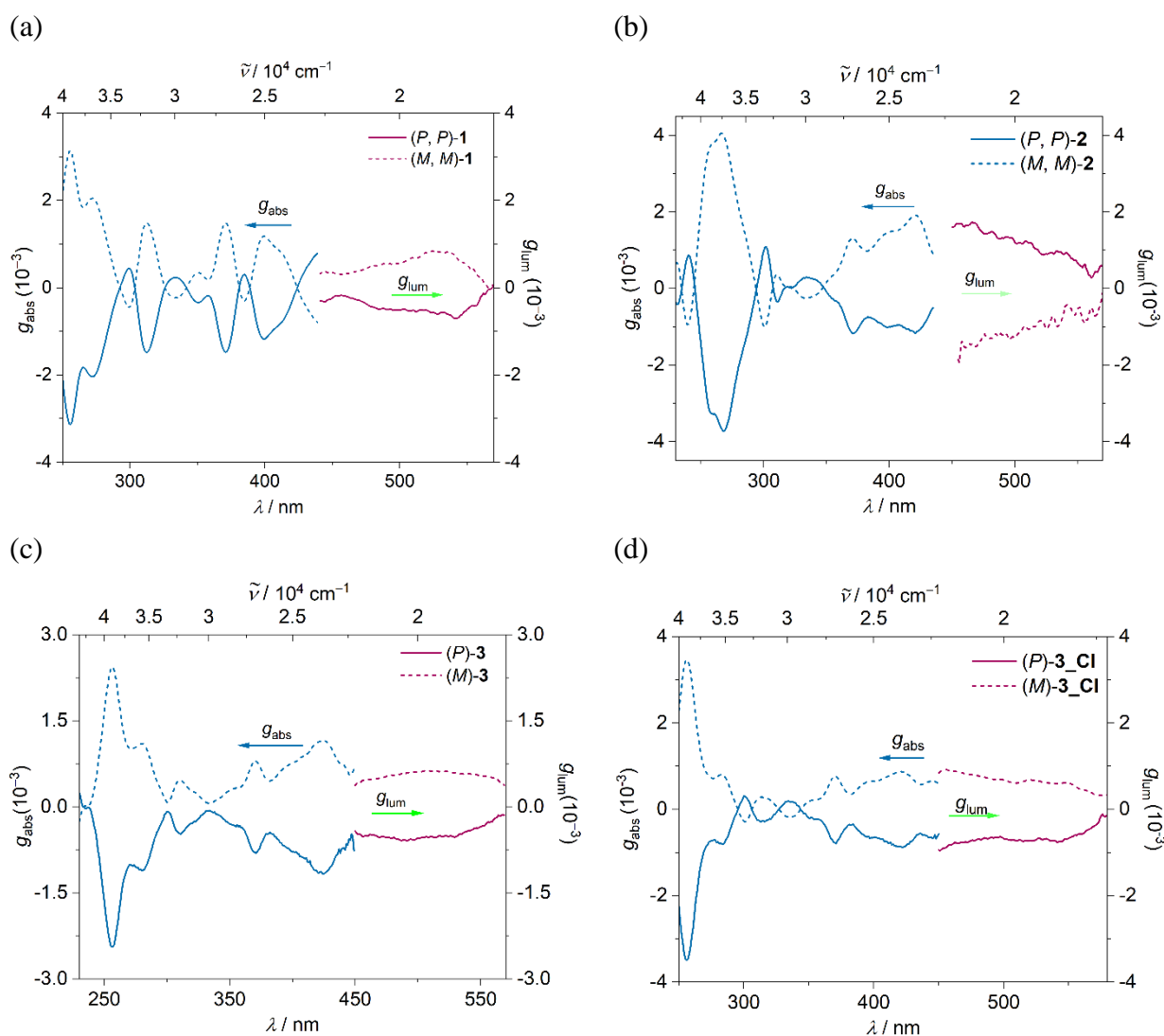
Figure S7. Absorption dissymmetry factor (g_{abs}) (blue) and luminescence dissymmetry factor (g_{lum}) (red) of enantiomers of (a) **1**, (b) **2**, (c) **3** and (d) **3_Cl** in dichloromethane (c ~10^{-5} M).

Table S3. Calculated electric and magnetic transition moments, and dissymmetry factor for $S_0 \rightarrow S_1$ and $S_1 \rightarrow S_0$ transitions.

Compound	$S_0 \rightarrow S_1$				$S_1 \rightarrow S_0$			
	$|\mu'|$ / 10^{-20} esu cm	$|m'|$ / 10^{-20} erg G^{-1}	$|\cos\theta'|$	$|g_{abs}|$ / 10^{-3}	$|\mu|$ / 10^{-20} esu cm	$|m|$ / 10^{-20} erg G^{-1}	$|\cos\theta|$	$|g_{lum}|$ / 10^{-3}
1	353.23	0.10	0.94	1.0	461.35	0.33	0.31	0.9
2	366.92	0.77	0.96	8.0	395.89	0.80	0.94	7.6
3	356.51	0.13	0.64	0.9	331.29	0.08	0.63	0.6

15

S6. Quantum chemical calculations

Conformational diastereomers: Hydrogen atoms and *tert*-butyl groups are omitted for clarity.

(a) Relative Gibbs's free energies and optimized geometries of diastereomers of **3Py**.
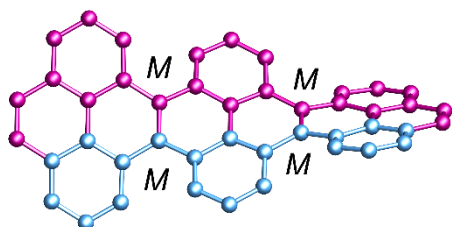
Helical-**3Py**
(0.56 kcal mol^{-1})
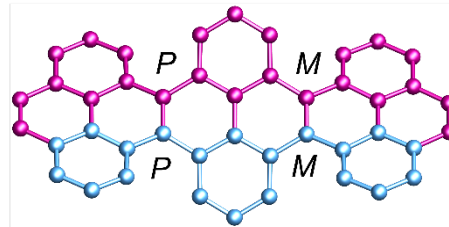
Waggling-**3Py**
(0.0 kcal mol^{-1})

(b) Relative Gibbs's free energies and optimized geometries of diastereomers of **1**.
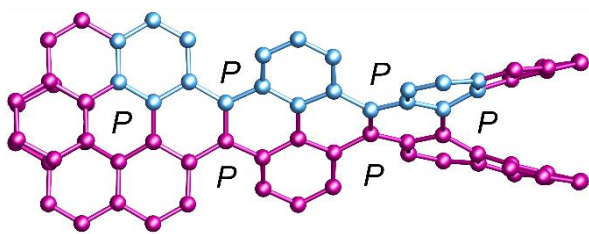
Right handed Helical
(*P,P*)-**1** (8.79 kcal mol^{-1})
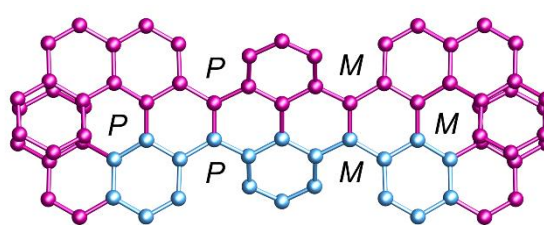
Waggling_2
(*P,M*)-**1** (5.91 kcal mol^{-1})
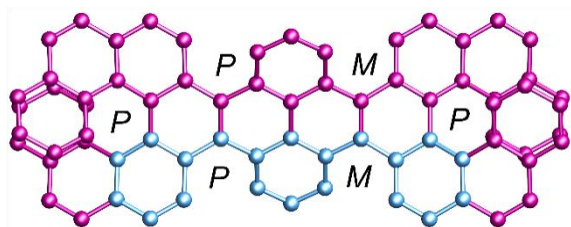
Waggling
(*P,P*)-**1** (4.38 kcal mol^{-1})
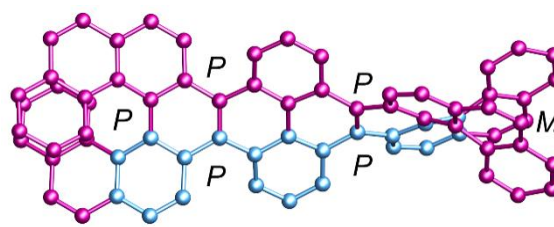
Helical
(*P,M*)-**1** (3.11 kcal mol^{-1})
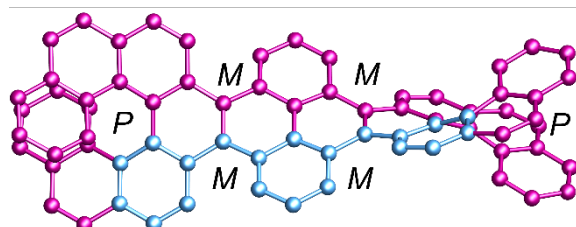
Left handed Helical
(*P,P*)-**1** (0.0 kcal mol^{-1})
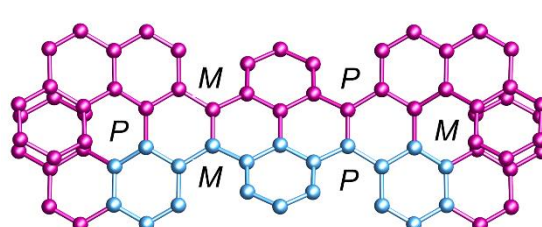
Waggling_1
(*P,M*)-**1** (0.0 kcal mol^{-1})

(c) Relative Gibbs's free energies and optimized geometries of diastereomers of (*P*)-**3**.
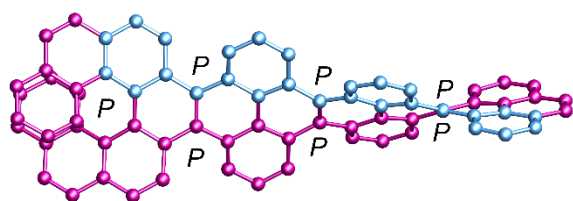
Right handed Helical
(*P*)-**3** (5.17 kcal mol^{-1})
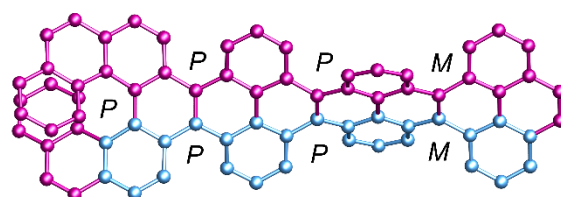
Waggling_4
(*P*)-**3** (5.16 kcal mol^{-1})
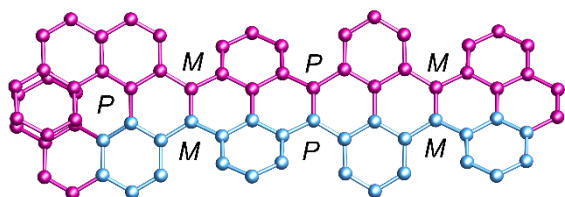
Waggling_3
(*P*)-**3** (2.54 kcal mol^{-1})
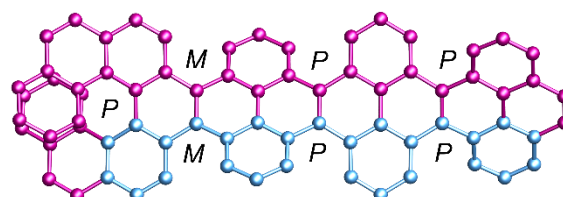
Waggling_2
(*P*)-**3** (2.50 kcal mol^{-1})
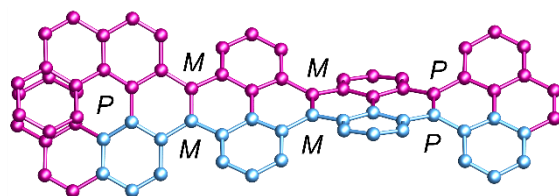
Waggling_1
(*P*)-**3** (1.91 kcal mol^{-1})
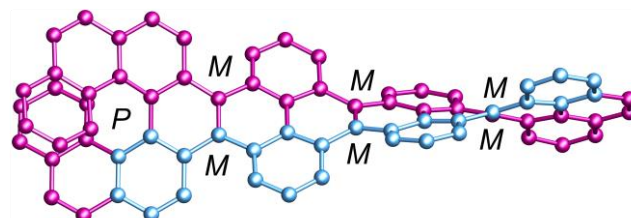
Left handed Helical
(*P*)-**3** (0.0 kcal mol^{-1})

(d) Relative Gibbs's free energies and optimized geometries of diastereomers of (*P*, *P*)-**2**.
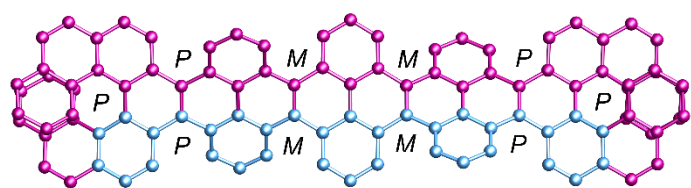
Waggling_6
(*P*,*P*)-**2** (13.29 kcal mol^{-1})
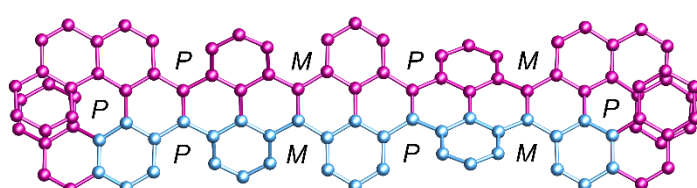
Waggling_5
(*P*,*P*)-**2** (12.23 kcal mol^{-1})
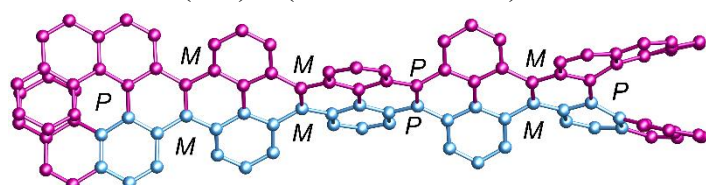
Waggling_4
(*P*,*P*)-**2** (11.15 kcal mol^{-1})
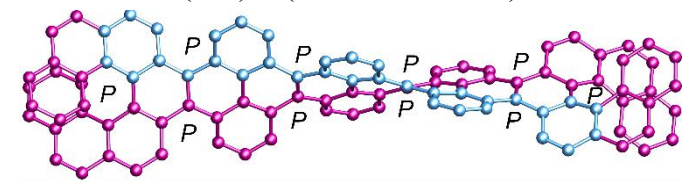
Right handed Helical
(*P*,*P*)-**2** (9.20 kcal mol^{-1})
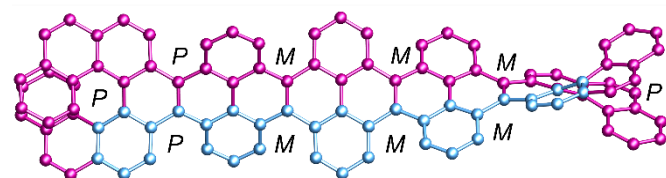
Waggling_3
(*P*,*P*)-**2** (6.98 kcal mol^{-1})
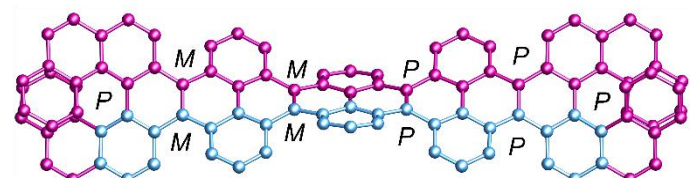
Waggling_2
(*P*,*P*)-**2** (6.71 kcal mol^{-1})
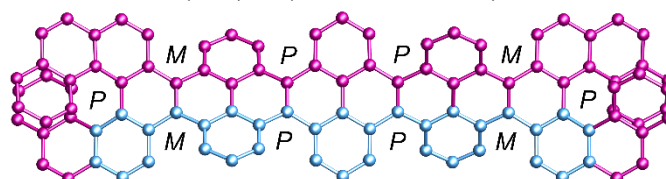
Waggling_1
(*P*,*P*)-**2** (4.37 kcal mol^{-1})
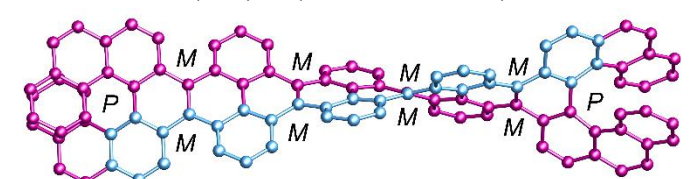
Left handed Helical
(*P*,*P*)-**2** (0.0 kcal mol^{-1})

(e) Relative Gibbs's free energies and optimized geometries of diastereomers of (*P*, *M*)-**2**.
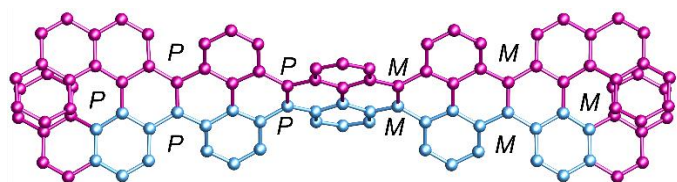
Waggling_6
(*P*,*M*)-**2** (7.51 kcal mol^{-1})
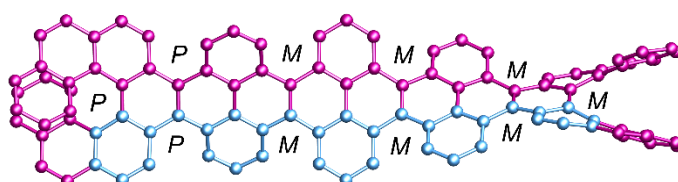
Waggling_5
(*P*,*M*)-**2** (6.79 kcal mol^{-1})
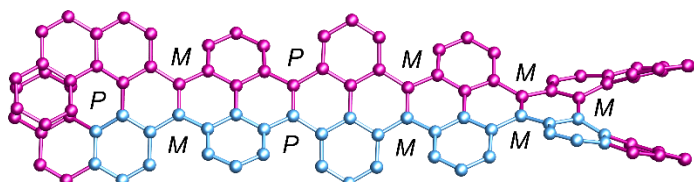
Waggling_4
(*P*,*M*)-**2** (4.34 kcal mol^{-1})
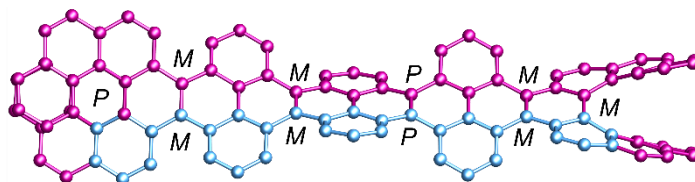
Waggling_3
(*P*,*M*)-**2** (4.04 kcal mol^{-1})
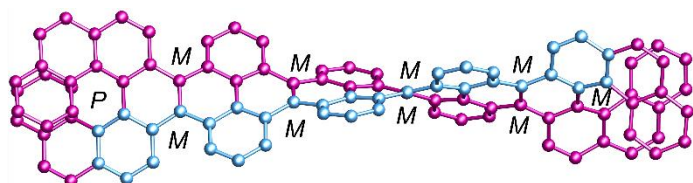
Helical
(*P*,*M*)-**2** (2.75 kcal mol^{-1})
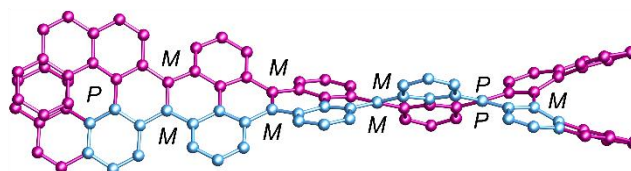
Waggling_2
(*P*,*M*)-**2** (0.38 kcal mol^{-1})
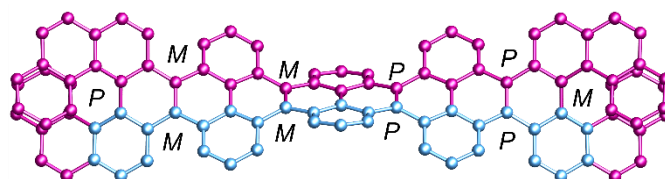
Waggling_1
(*P*,*M*)-**2** (0.0 kcal mol^{-1})

Table S4. Frontier molecular orbitals of **1**, **2** and **3** (isosurface value 0.02). Hydrogen atoms are omitted for clarity.
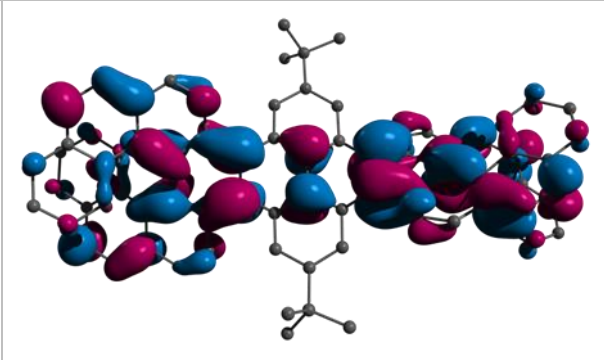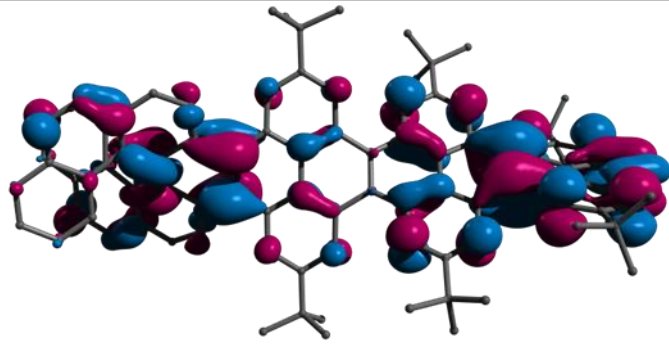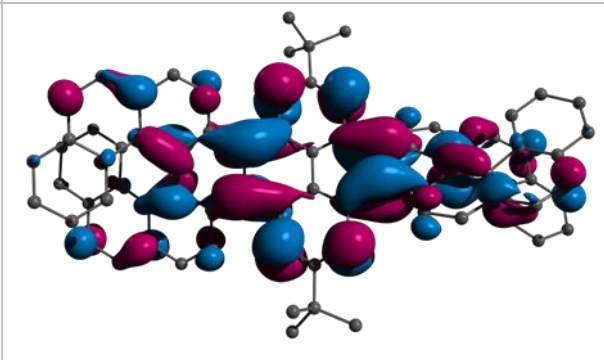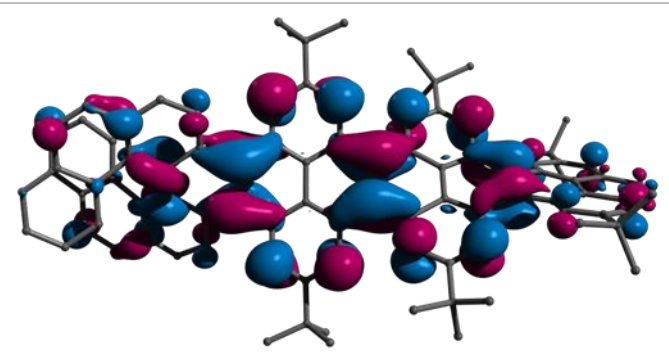
FMOs	1	3
LUMO+1		
LUMO		
HOMO		
HOMO−1		
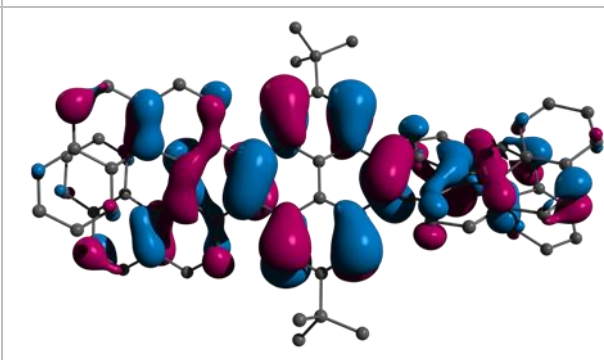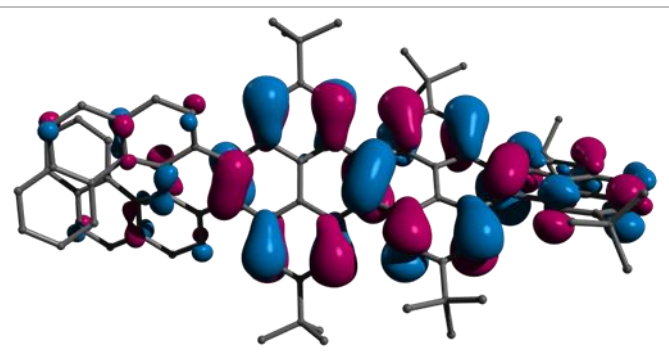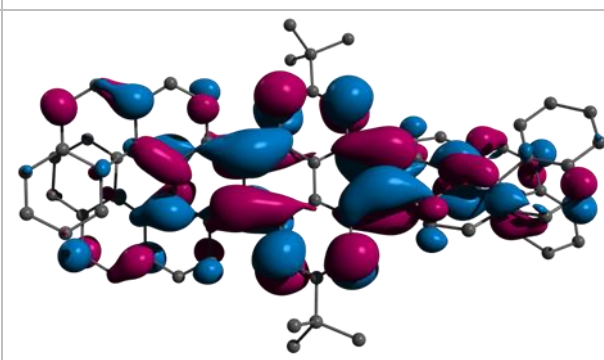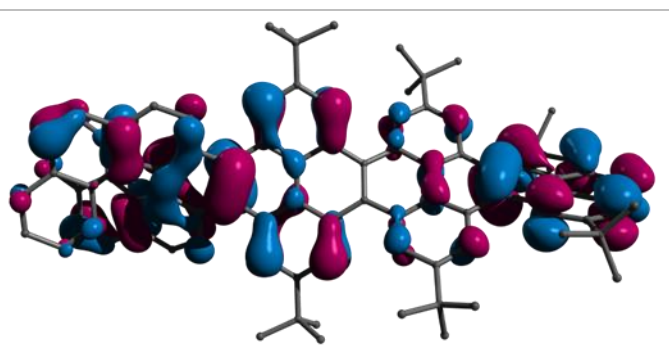
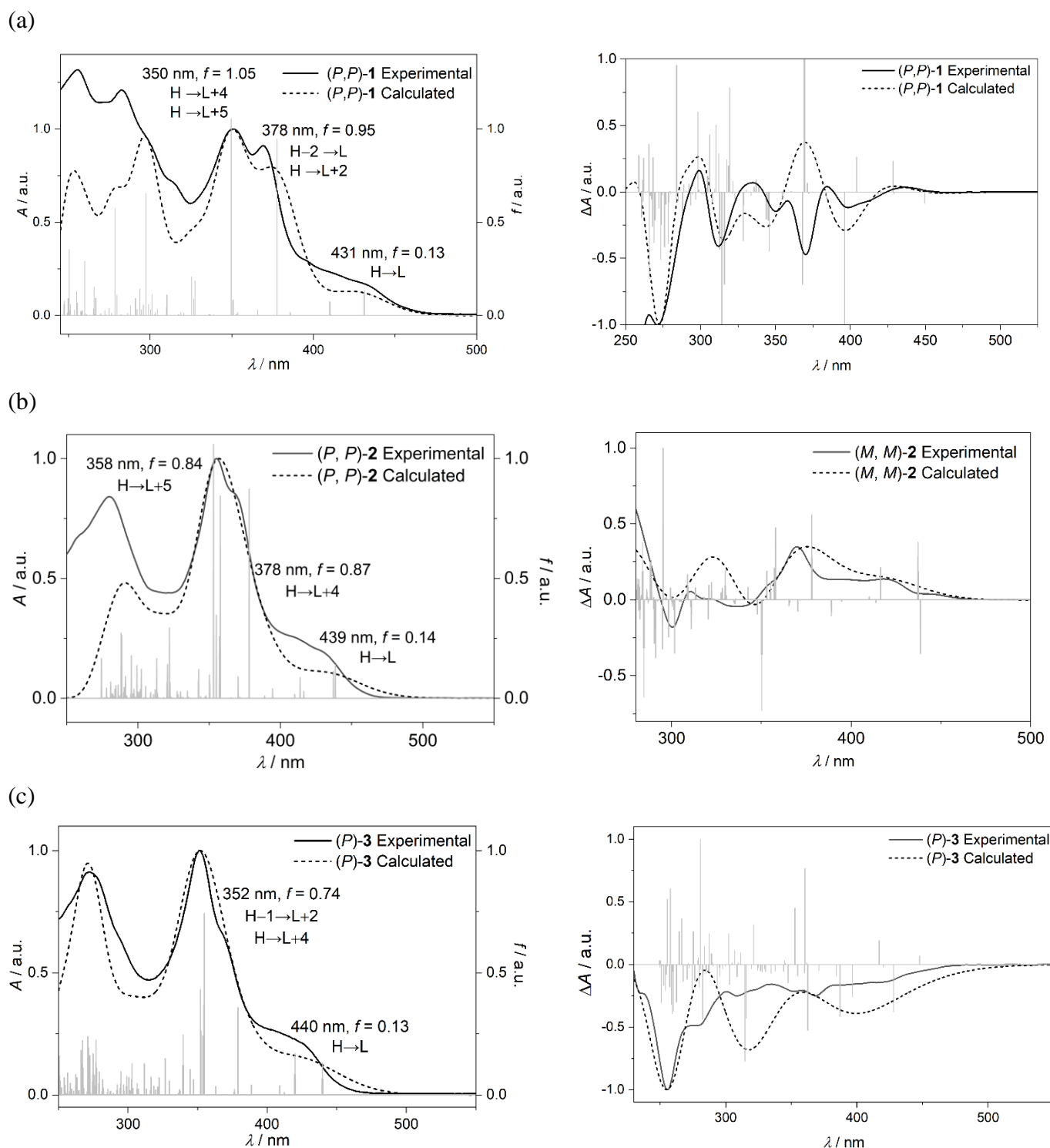| FMOs	2
LUMO+1	
LUMO	
HOMO	
HOMO−1	

(a)

(b)

(c)
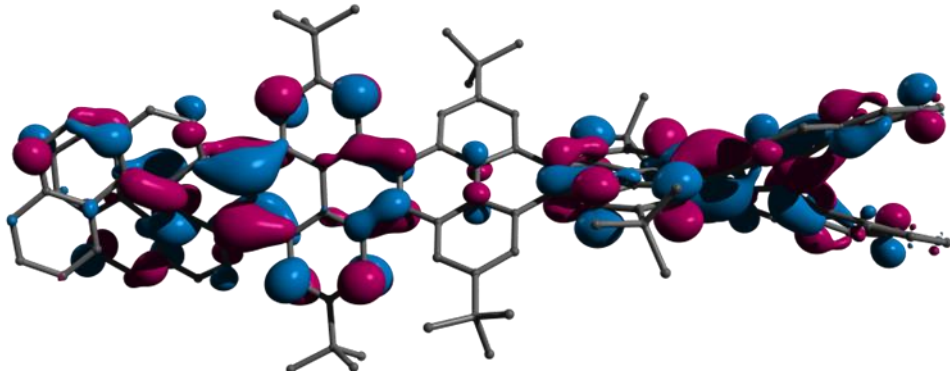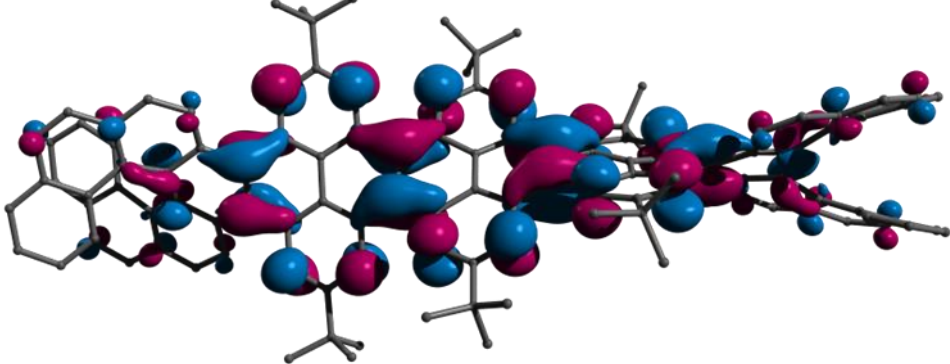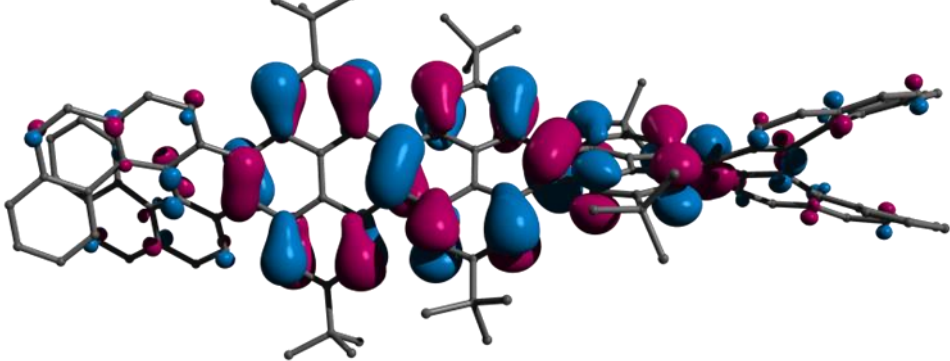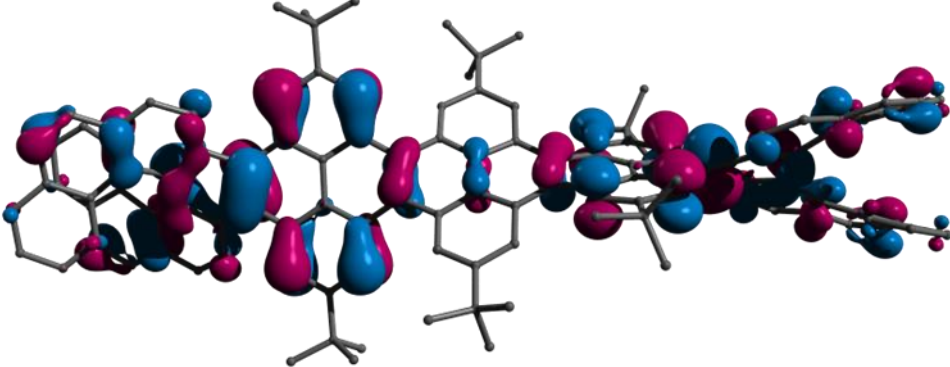
Figure S8. Comparison of experimental (solid) and TD-DFT calculated (dashed) UV–Vis absorption (left) and ECD spectra (right) of (a) (*P*, *P*)-**1** (shifted by 0.09 eV, 14 nm), (b) (*P*, *P*)-**2** (shifted by 0.09 eV, 15 nm) and (c) (*P*)-**3** (shifted by 0.08 eV, 13 nm) along with assignments of key transitions. H = HOMO, L = LUMO, *f* = oscillator strength.

Table S5a. Summary of TD-DFT calculated key low energy transitions of **1**.

Excited singlet state	Wavelength / nm	Energy / eV	Major transitions	Contribution	Oscillator strength (f)
1	431	2.87	HOMO→LUMO	0.69	0.13
2	378	3.28	HOMO–2→LUMO	0.51	0.95
			HOMO→LUMO+2	0.41	
3	350	3.54	HOMO→LUMO+4	0.53	1.05
			HOMO→LUMO+5	0.24	

Table S5b. Summary of TD-DFT calculated key low energy transitions of **2**.

Excited singlet state	Wavelength / nm	Energy / eV	Major transitions	Contribution	Oscillator strength (f)
1	439	2.82	HOMO→LUMO	0.68	0.14
9	378	3.28	HOMO→LUMO+4	0.44	0.87
			HOMO–3→LUMO	0.31	
15	358	3.46	HOMO→LUMO+5	0.34	0.84
			HOMO–1→LUMO+3	0.31	
19	353	3.51	HOMO–1→LUMO	0.36	1.06
			HOMO→LUMO+6	0.28	

Table S5c. Summary of TD-DFT calculated key low energy transitions of **3**.

Excited singlet state	Wavelength / nm	Energy / eV	Major transitions	Contribution	Oscillator strength (f)
1	440	2.82	HOMO→LUMO	0.67	0.13
6	379	3.27	HOMO–2→LUMO	0.47	0.36
10	352	3.52	HOMO→LUMO+4	0.28	0.74
			HOMO–1→LUMO+2	0.41	

NICS calculations: The Nucleus Independent Chemical Shift (NICS) calculations were performed on ωB97XD/6-31G(d,p) optimized geometry at GIAO-B3LYP/6-311+G(2d,p) level. Considering the non-planarity of molecules, the NICS(1)$_{ZZ}$ values were obtained by placing dummy atom at 1 Å above and below the each ring.

(P, P)-**1** $\qquad\qquad$ (P, M)-**1**

Table S6a. The calculated NICS(0) and NICS(1)$_{ZZ}$ values for (P, P)-**1** and (P, M)-**1** .

Ring	(P, P)-**1**			(P, M)-**1**		
	NICS(1)$_{ZZ}$ (Up)	NICS(1)$_{ZZ}$ (Down)	NICS(0) iso	NICS(1)$_{ZZ}$ (Up)	NICS(1)$_{ZZ}$ (Down)	NICS(0) iso
A	−29.54	−32.46	−9.29	−32.30	−34.16	−9.39
B	−20.89	−20.58	−5.13	−21.88	−21.45	−5.17
C	−15.63	−9.55	−5.05	−18.68	−12.11	−4.98
D	−9.55	−4.52	−1.01	−7.82	−7.82	−1.01
E	−5.83	−5.84	0.57	−3.13	−3.17	1.18
F	−26.33	−26.57	−8.33	−21.53	−28.70	−8.18
G				−3.17	−3.13	1.18
H				−7.81	−7.81	−1.01
I				−18.71	−12.09	−4.98
J				−21.90	−21.47	−5.19
K				−32.11	−34.11	−9.37

(P, P)-2   (P, M)-2

Table S6b. The calculated NICS(0) and NICS(1)$_{ZZ}$ values for (P, P)-**2** and (P, M)-**2**.

Ring	(P, P)-**2**			(P, M)-**2**		
	NICS(1)$_{ZZ}$ (Up)	NICS(1)$_{ZZ}$ (Down)	NICS(0) iso	NICS(1)$_{ZZ}$ (Up)	NICS(1)$_{ZZ}$ (Down)	NICS(0) iso
A	−11.99	−14.24	−9.37	−27.09	−30.49	−9.31
B	−10.76	−9.28	−5.24	−19.59	−19.17	−5.05
C	−3.15	−1.96	−4.94	−13.37	−7.75	−4.95
D	2.08	1.37	−1.09	−2.88	−3.04	−1.05
E	−2.90	−3.39	1.58	−4.55	−14.55	1.19
F	−20.29	−14.09	−8.23	−26.67	−24.69	−8.23
G	−3.79	−3.83	0.61	−5.29	−5.19	0.98
H	−5.94	−6.18	1.04	−1.32	−1.25	1.23
I	−26.99	−26.88	−8.26	−13.26	−24.02	−8.13
J				−1.20	−1.10	1.30
K				−6.07	−6.11	0.66
L				−26.71	−24.84	−8.21
M				−3.65	−3.72	1.53
N				−3.31	−3.33	−1.13
O				−13.71	−8.01	−4.94
P				−19.69	−19.34	−5.01
Q				−27.51	−30.91	−9.32
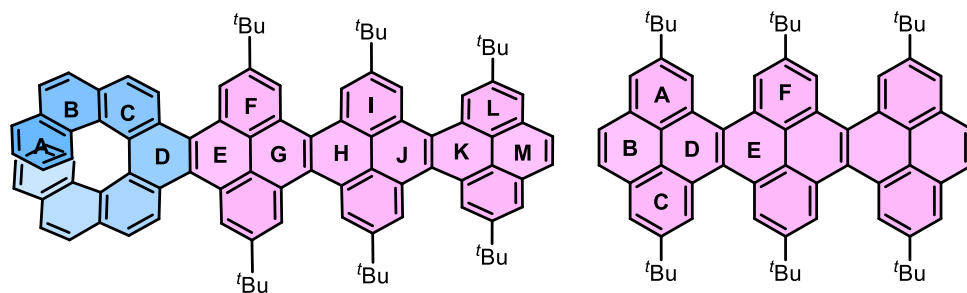
Table S6c. The calculated NICS(0) and NICS(1)$_{ZZ}$ values for (*P*)-**3** and **3Py**.

Ring	(*P*)-**3**			**3Py**		
	NICS(1)$_{ZZ}$ (Up)	NICS(1)$_{ZZ}$ (Down)	NICS(0) iso	NICS(1)$_{ZZ}$ (Up)	NICS(1)$_{ZZ}$ (Down)	NICS(0) iso
A	−11.96	−14.05	−9.35	−26.37	−30.95	−9.40
B	−10.87	−9.22	−5.22	−14.56	−14.56	−2.92
C	−3.26	−1.85	−4.99	−30.95	−26.36	−9.40
D	1.92	1.51	−1.02	−4.04	−4.04	1.36
E	−3.66	−3.88	1.20	−2.74	−2.74	0.99
F	−20.39	−14.34	−8.29	−26.07	−16.19	−8.32
G	−3.28	−3.23	0.88			
H	−6.07	−6.06	1.01			
I	−26.90	−27.24	−8.31			
J	−6.14	−6.51	0.86			
K	−3.45	−3.36	0.58			
L	−15.26	−23.35	−9.54			
M	−7.63	−8.11	−1.99			

S7. X-Ray crystallography

The single crystals were grown by slow diffusion of hexane (HPLC grade) to solution of (*P*, *P*)-**1** and **3Py** in DCM (HPLC grade) in a NMR tube. Crystallographic data have been deposited with the Cambridge Crystallographic Data Centre as supplementary publication no. CCDC 2315652 and 2315653. These data can be obtained free of charge from the Cambridge Crystallographic Data Centre via www.ccdc.ac.uk/data.request/cif.

(a)
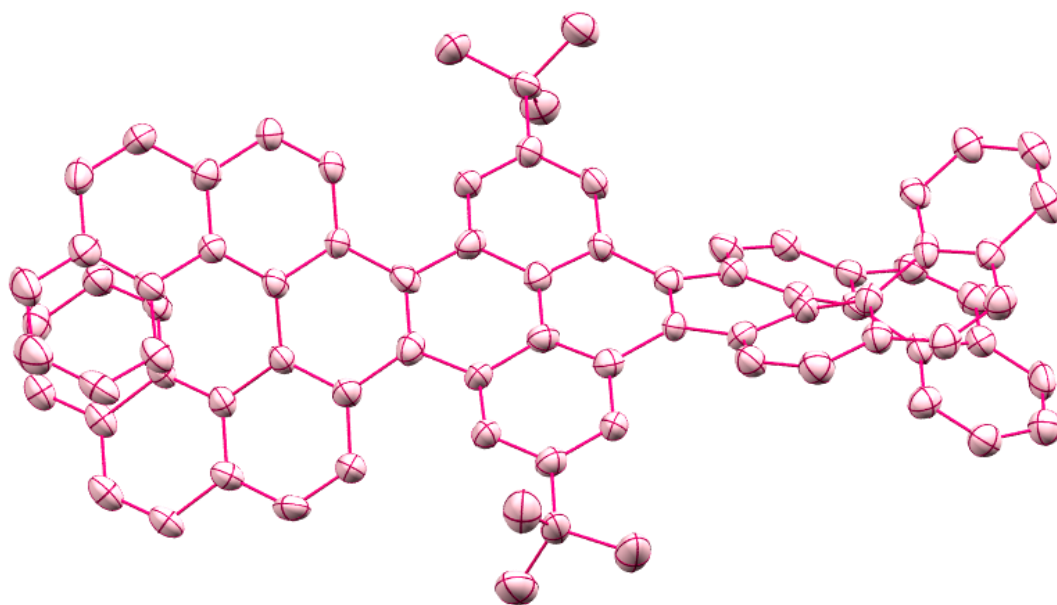
(b)
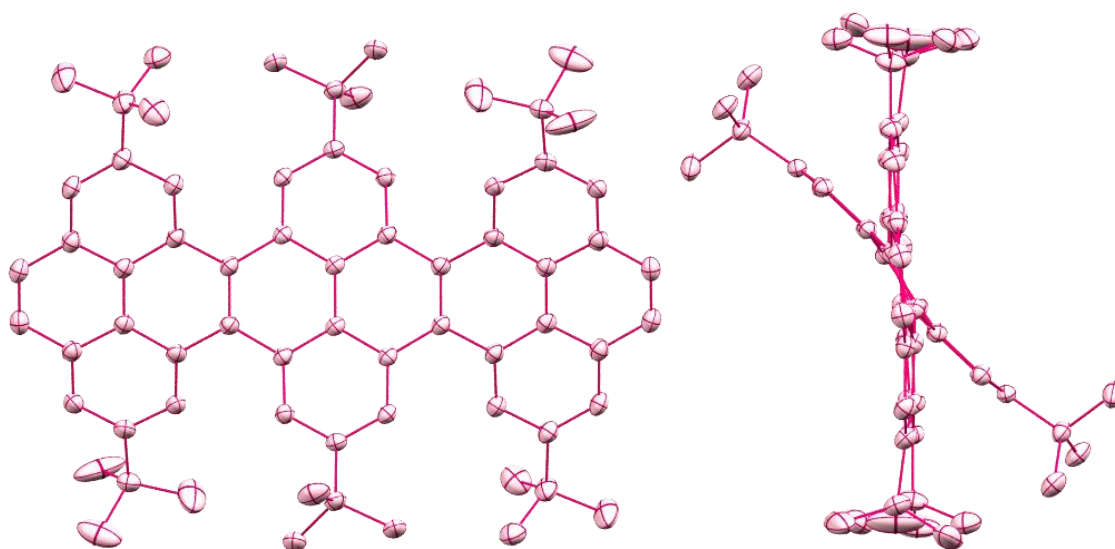
Figure S9. ORTEP diagram of (a) (*P*, *P*)-**1** and (b) **3Py**. Thermal ellipsoids are shown at the 50% probability level. Hydrogen atoms are omitted for clarity.

Table S7. Crystallographic table for (*P*, *P*)-**1** and **3Py**.

Data	(*P*, *P*)-**1**	**3Py**
CCDC	2315653	2315652
Empirical formula	$C_{83}H_{60}Cl_6$	$C_{70}H_{74}Cl_4$
Formula weight (g·mol^{-1})	1270.01	1057.09
Temperature (K)	100.01(10)	100(2)
Radiation, λ (Å)	Cu$_{Kα}$, 1.54184	Cu$_{Kα}$, 1.54184
Crystal system	triclinic	triclinic
Space group	*P*1	*P*$\bar{1}$
Unit cell dimensions		
a (Å)	14.6922(4)	14.16160(10)
b (Å)	15.4658(4)	14.61250(10)
c (Å)	16.5251(4)	15.92860(10)
α (°)	114.189(3)	66.4050(10)
β (°)	109.595(3)	76.5680(10)
γ (°)	93.418(2)	74.1110(10)
Volume (Å^3)	3140.90(17)	2876.94(4)
Z	2	2
Calculated density (Mg·m^{-3})	1.343	1.220
Absorption coefficient (mm^{-1})	2.862	
F(000)	1320	1124
Theta range for collection	3.191 to 73.493°	3.057 to 75.002°
Reflections collected	31564	123212
Independent reflections	31564	11428
Minimum/maximum transmission	0.64500/1.00000	0.675/1.000
Refinement method	Full-matrix least-squares on F^2	Full-matrix least-squares on F^2
Data / parameters / restraints	31564 / 1648 / 235	11428 / 687 / 413
Goodness-of-fit on F^2	1.052	1.072
Final R indices [I>2σ(I)]	R$_1$ = 0.0936, *w*R$_2$ = 0.2424	R$_1$ = 0.0643, *w*R$_2$ = 0.1687
R indices (all data)	R$_1$ = 0.1143, *w*R$_2$ = 0.2691	R$_1$ = 0.0671, *w*R$_2$ = 0.1710
Maximum/minimum residual electron density (e·Å^{-3})	0.831 / –0.807	1.170 / –1.228
Flack parameter	0.003(19)	

For (*P*, *P*)-**1**: Structure was refined as two component twins. Solvent molecules (dichloromethane) were fitted to idealized geometry. Two of these molecules showed positional disordered. Atomic displacement parameters (ADPs) off all disordered atoms were restraint with similarity restraint (SIMU), rigid-body restraint (RIGU) and isotropic restraint (ISOR).

For **3Py**: Two tert-butyl groups were rotationally disordered. The displacement parameters of opposite atoms belonging to these groups were constrained to each other with EADP keyword. Additionally, all ADPs were restraint with RIGU keyword in ShelXL input ('enhanced rigid bond' restraint for all bonds in the connectivity list), similarity restraint SIMU and their U_{ii} parameters were restrained with ISOR keyword to approximate isotropic behavior.

S8. NMR spectroscopy
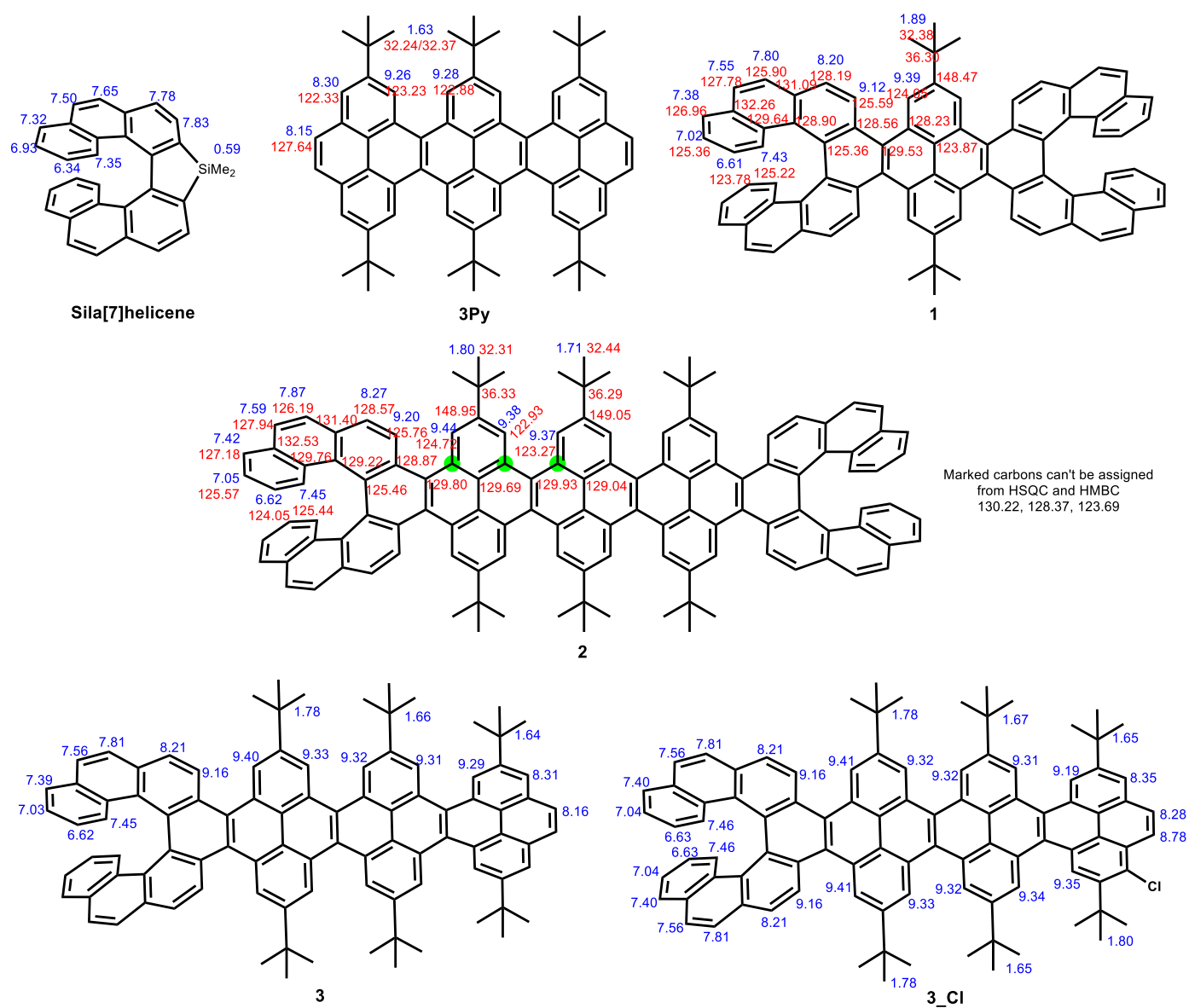
Figure S10. ^{1}H (blue) and ^{13}C NMR (red) peaks assigned to respective atoms in discussed molecules.
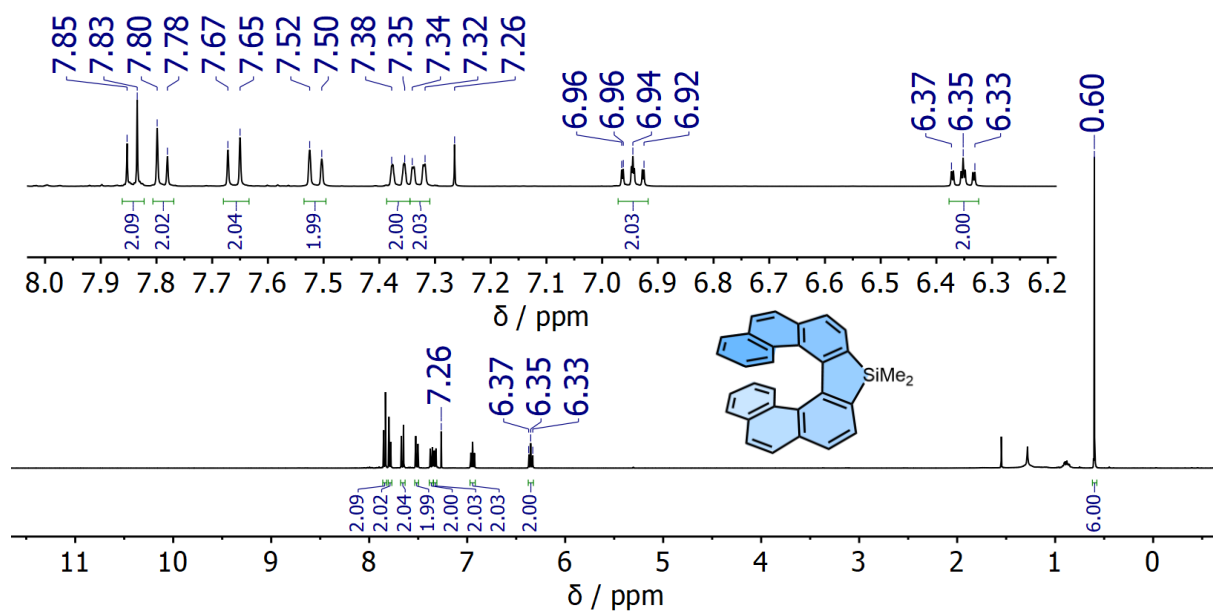
Figure S11. ^{1}H NMR spectrum of (*P*)-**Dimethylsila[7]helicene** (400 MHz, CDCl$_3$).
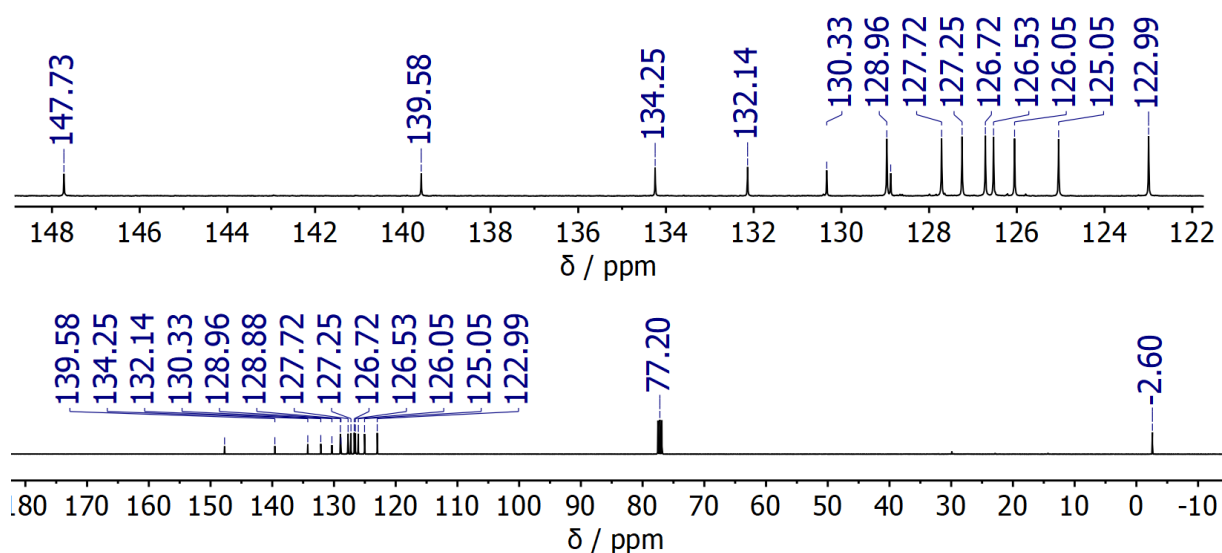
Figure S12. ^{13}C(^{1}H) NMR spectrum of (*P*)- **Dimethylsila[7]helicene** (101 MHz, CDCl$_3$).
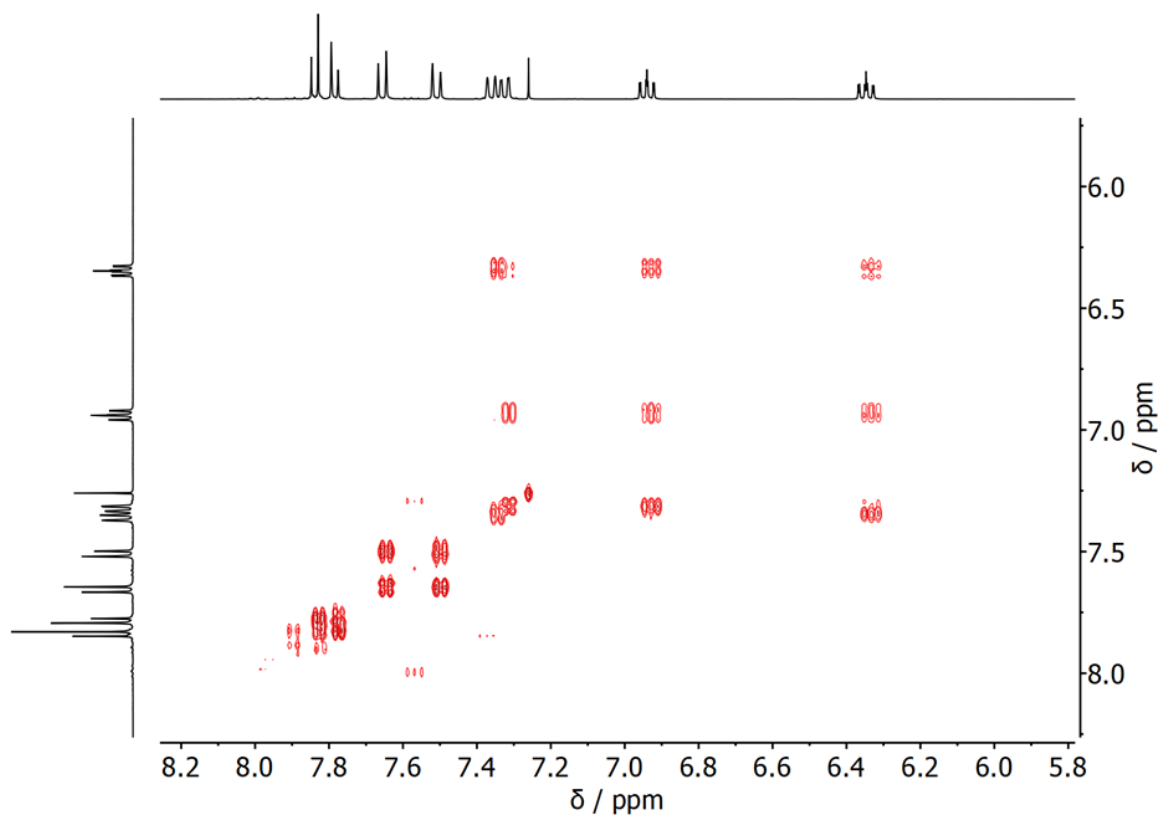
Figure S13. ^{1}H – ^{1}H COSY NMR spectrum of (*P*)-**Dimethylsila[7]helicene** (400 MHz, CDCl$_3$).
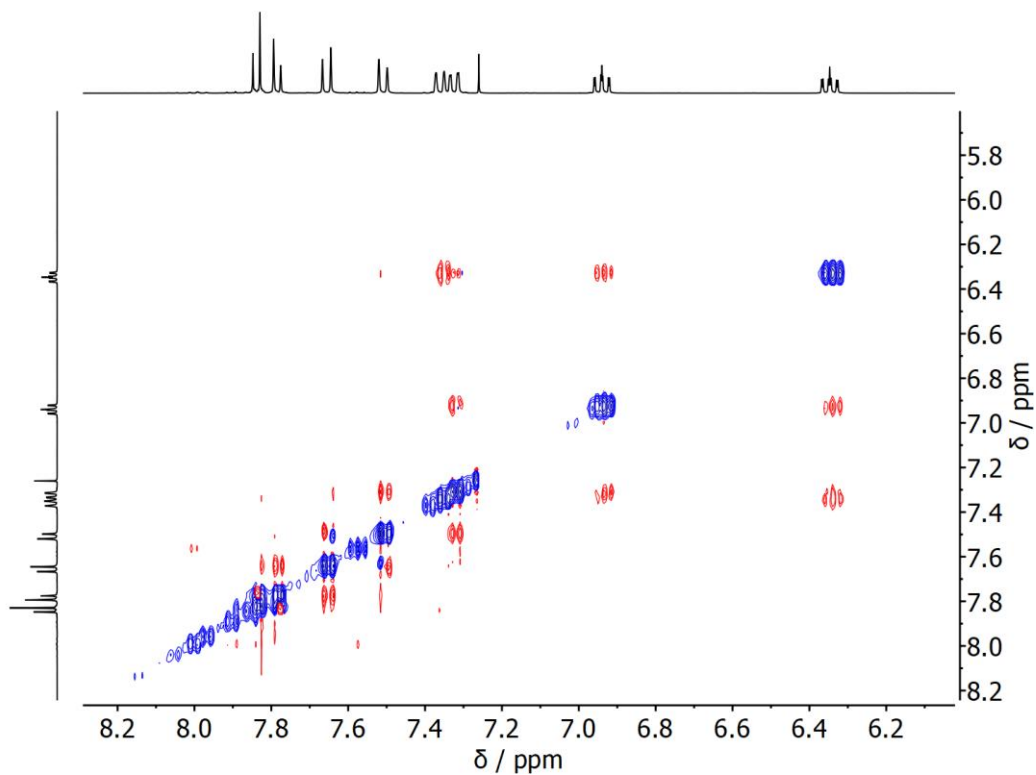
Figure S14. ^{1}H – ^{1}H NOESY NMR spectrum of (*P*)- **Dimethylsila[7]helicene** (400 MHz, CDCl$_3$).
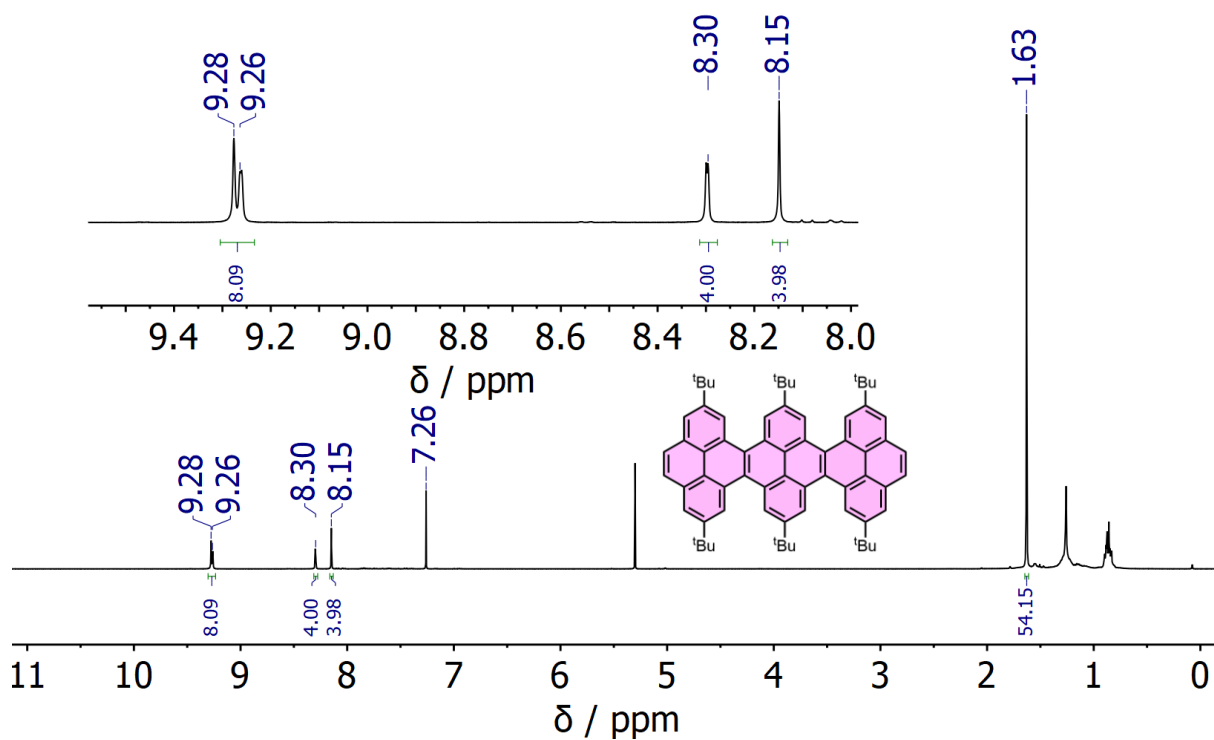
Figure S15. ^{1}H NMR spectrum of **3Py** (400 MHz, CDCl$_3$).
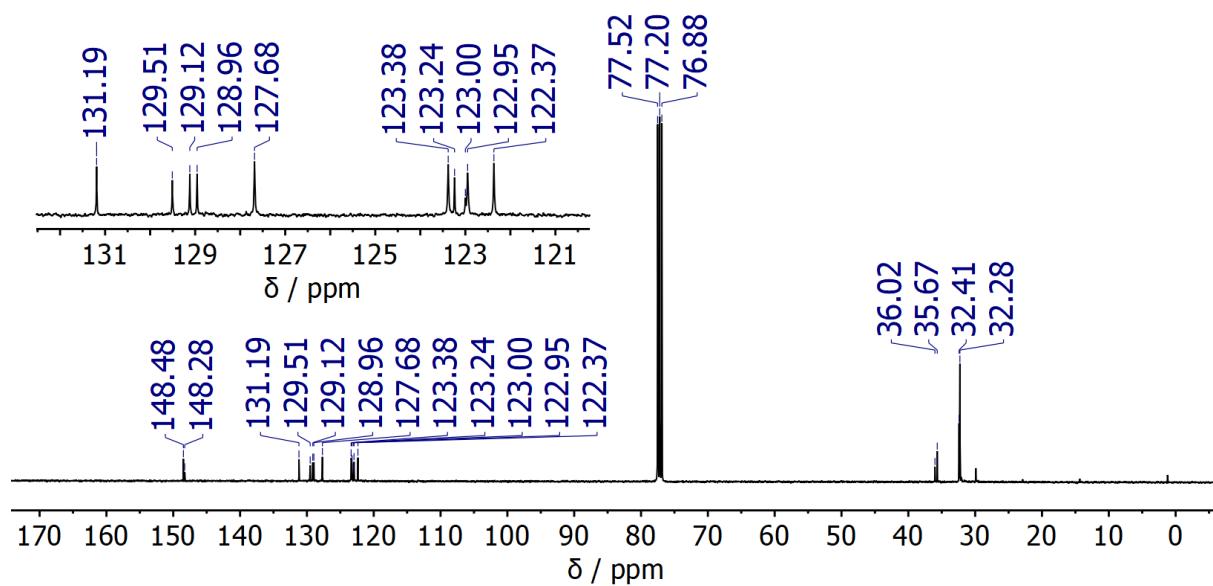
Figure S16. ^{13}C(^{1}H) NMR spectrum of **3Py** (101 MHz, CDCl$_3$).

32
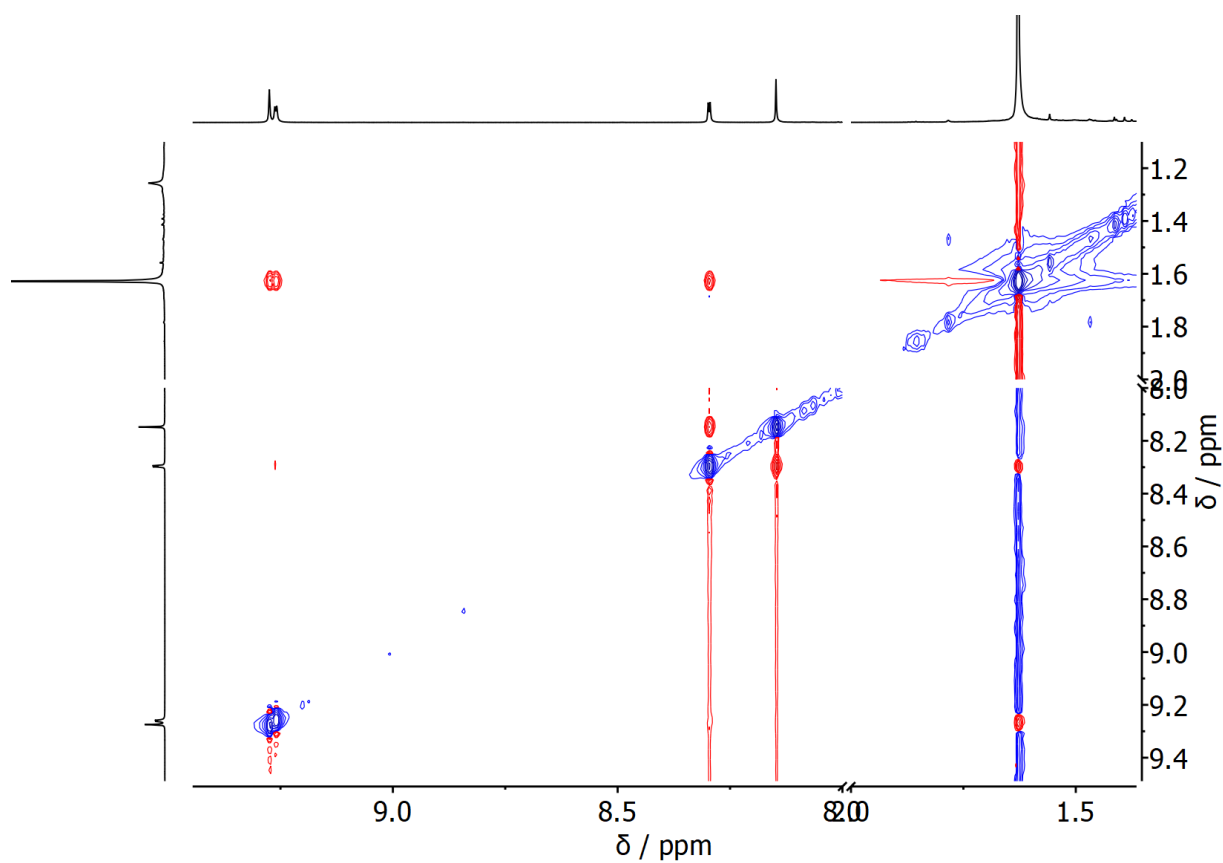
Figure S17. $^1H – {}^1H$ NOESY NMR spectrum of **3Py** (400 MHz, CDCl$_3$).
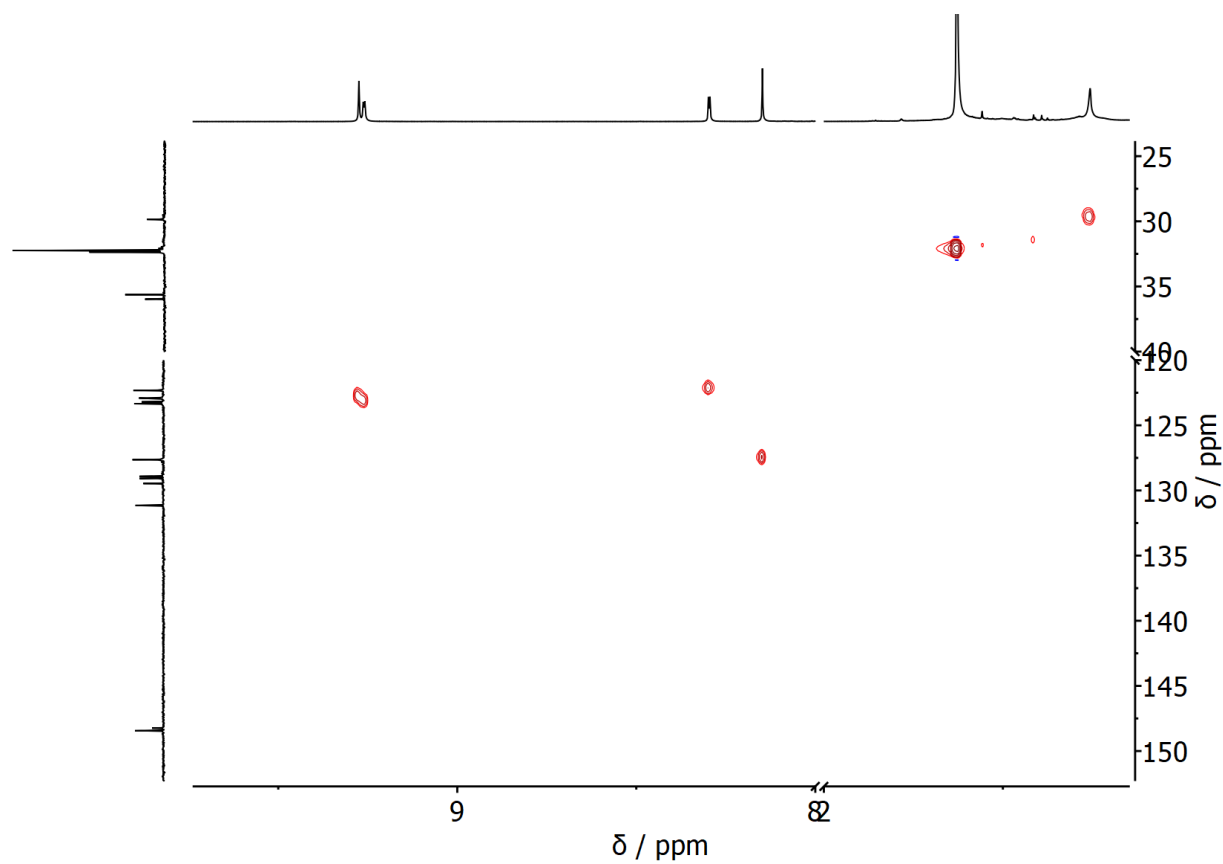
Figure S18. $^1H – {}^{13}C$ HSQC NMR spectrum of **3Py** (400 MHz, CDCl$_3$).
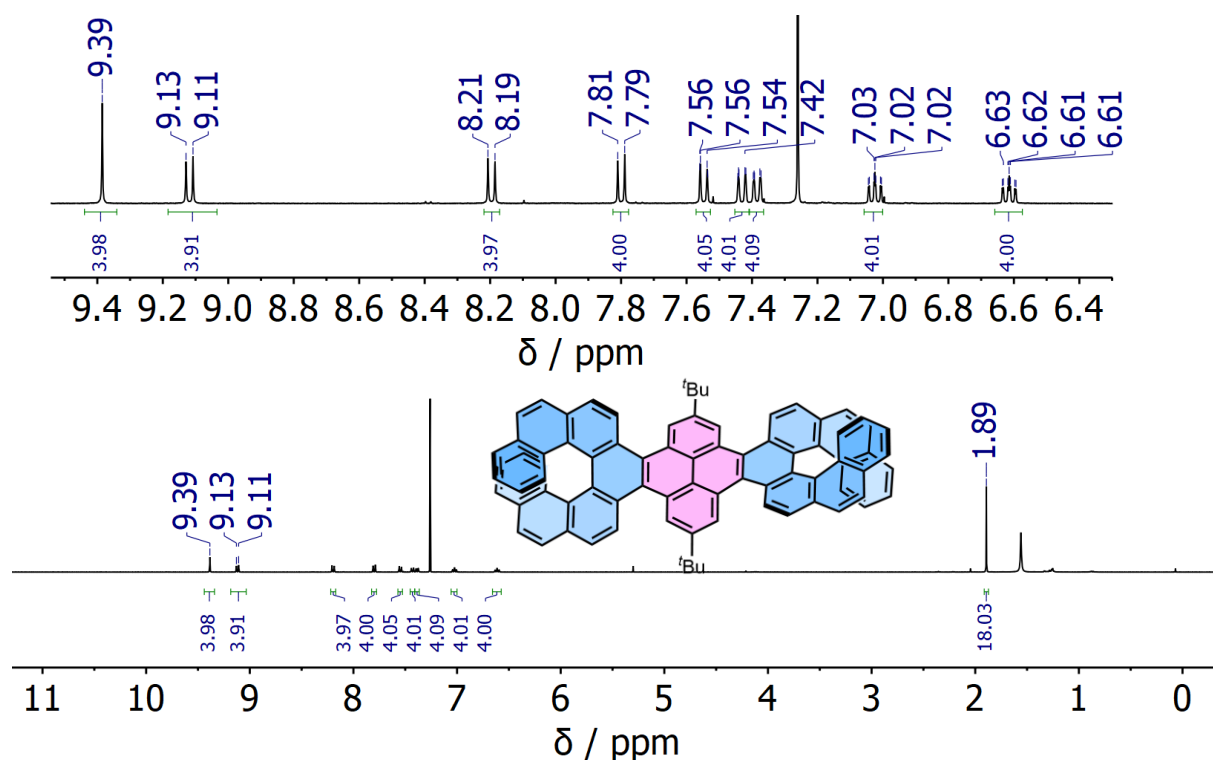
Figure S19. ^{1}H NMR spectrum of (*P, P*)-**1** (400 MHz, CDCl$_3$).
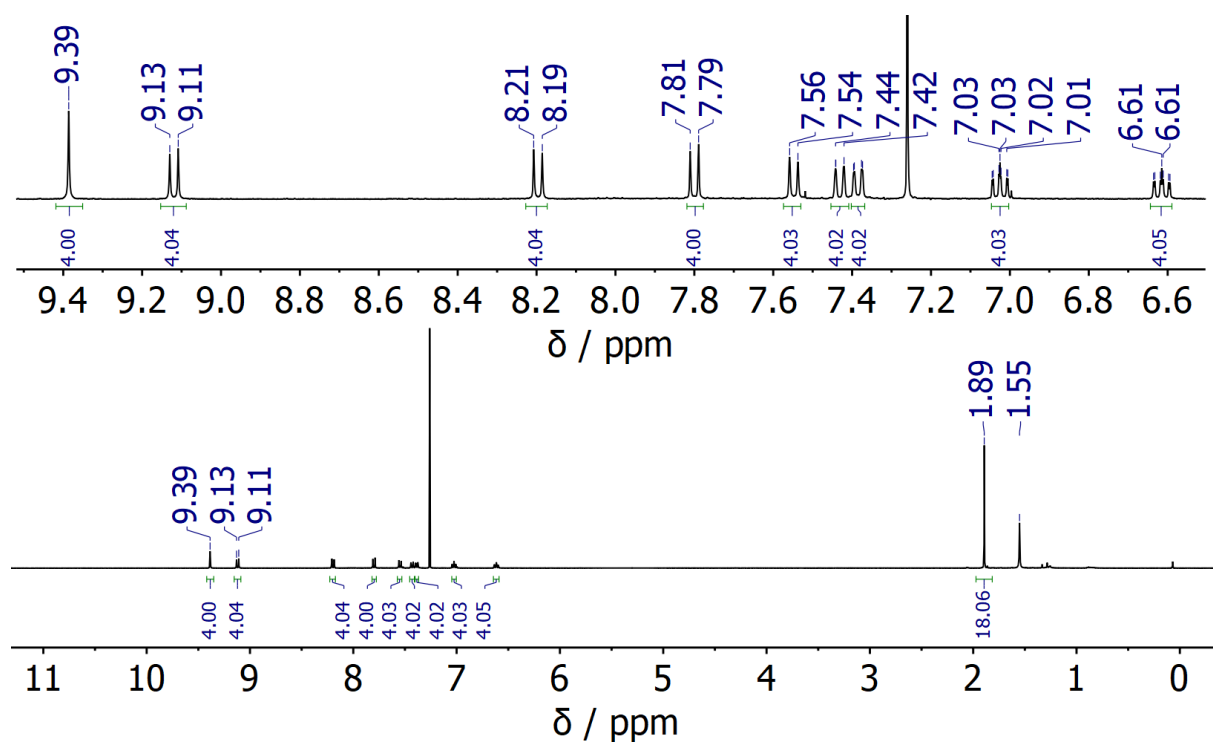
Figure S20. ^{1}H NMR spectrum of (*P, M*)-**1** (400 MHz, CDCl$_3$).
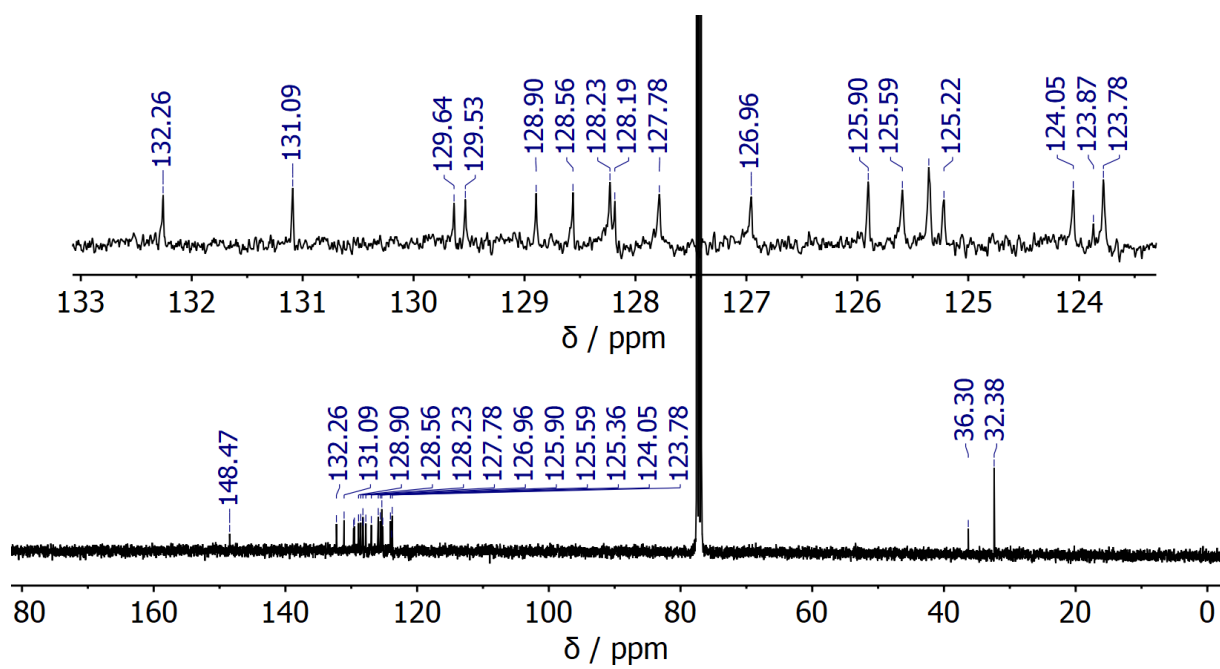
Figure S21. $^{13}C\{^{1}H\}$ NMR spectrum of (P, P)-**1** (101 MHz, CDCl$_3$).
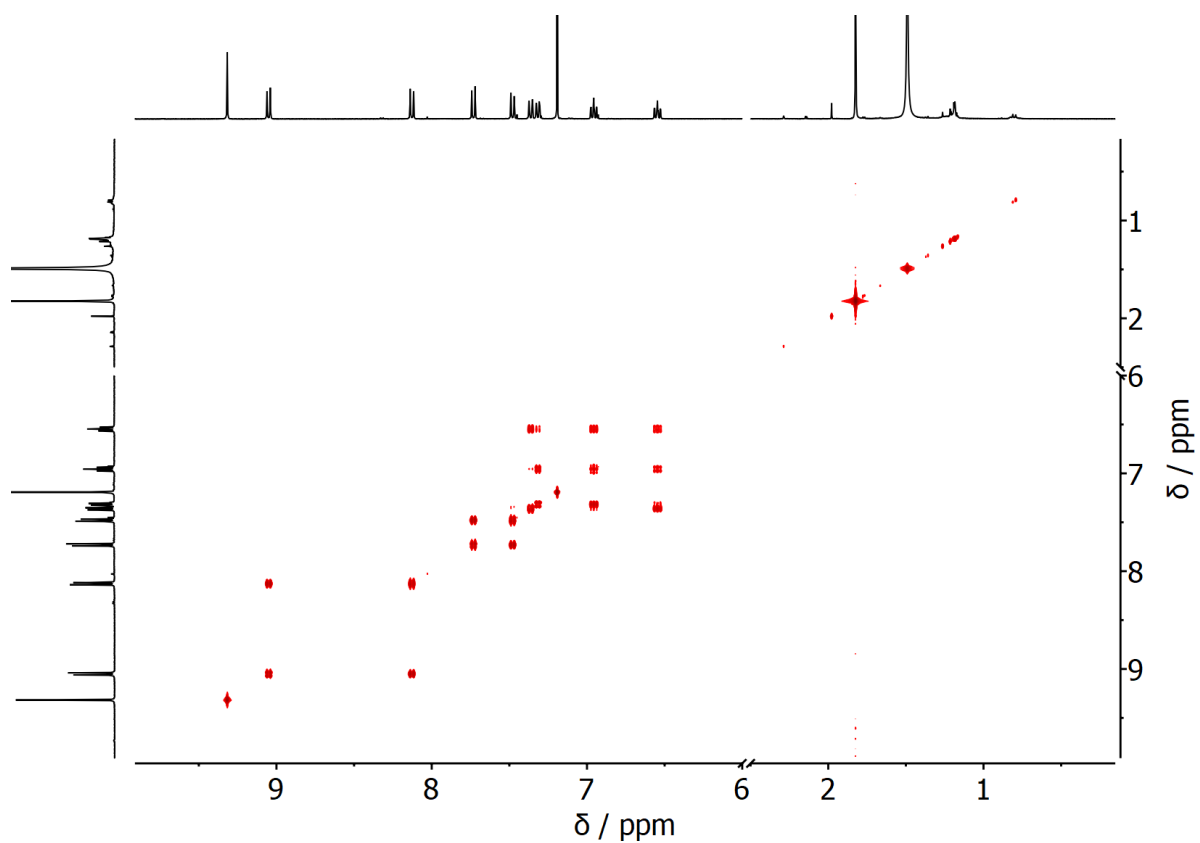
Figure S22. ^1H – ^1H COSY NMR spectrum of (*P*, *P*)-**1** (400 MHz, CDCl$_3$).
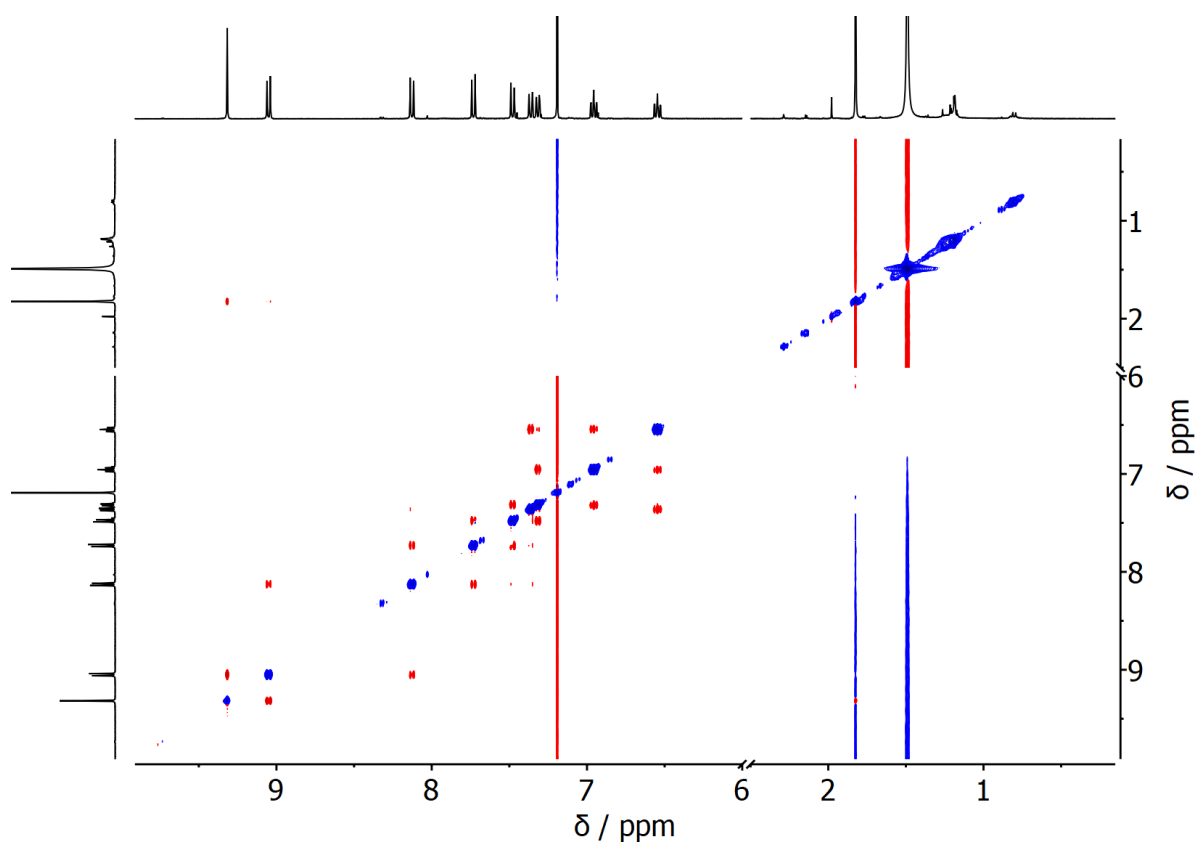
Figure S23. ^1H – ^1H NOESY NMR spectrum of (*P*, *P*)-**1** (400 MHz, CDCl$_3$).
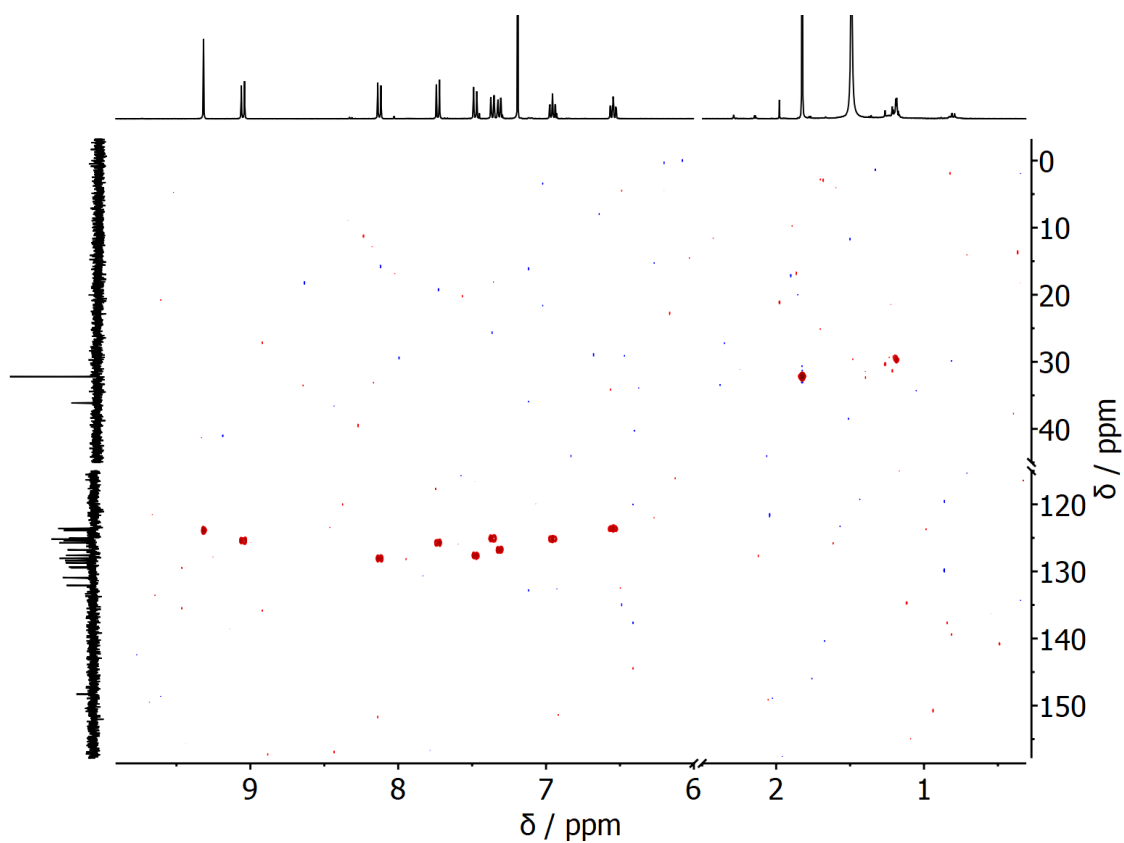
Figure S24. $^{1}H – ^{13}C$ HSQC NMR spectrum of (*P, P*)-**1** (400 MHz, CDCl$_3$).
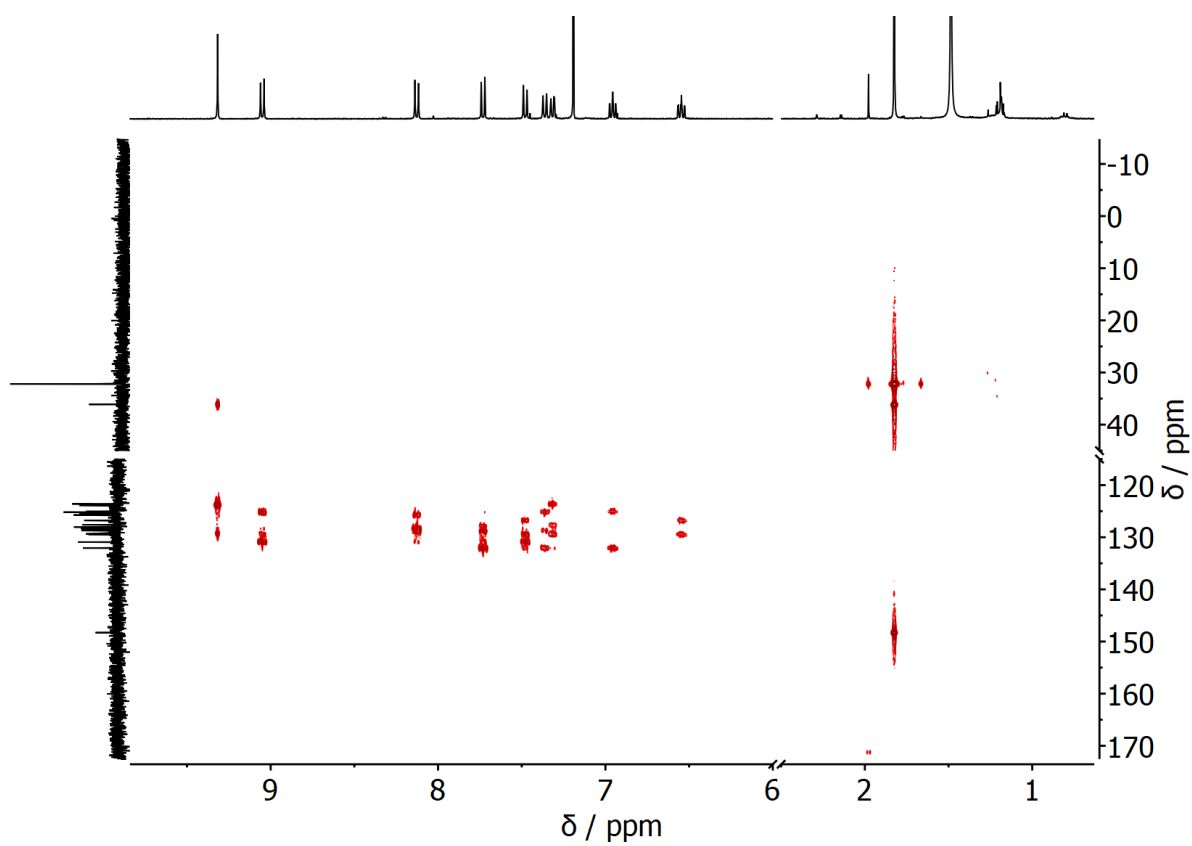
Figure S25. $^{1}H – ^{13}C$ HMBC NMR spectrum of (*P, P*)-**1** (400 MHz, CDCl$_3$).
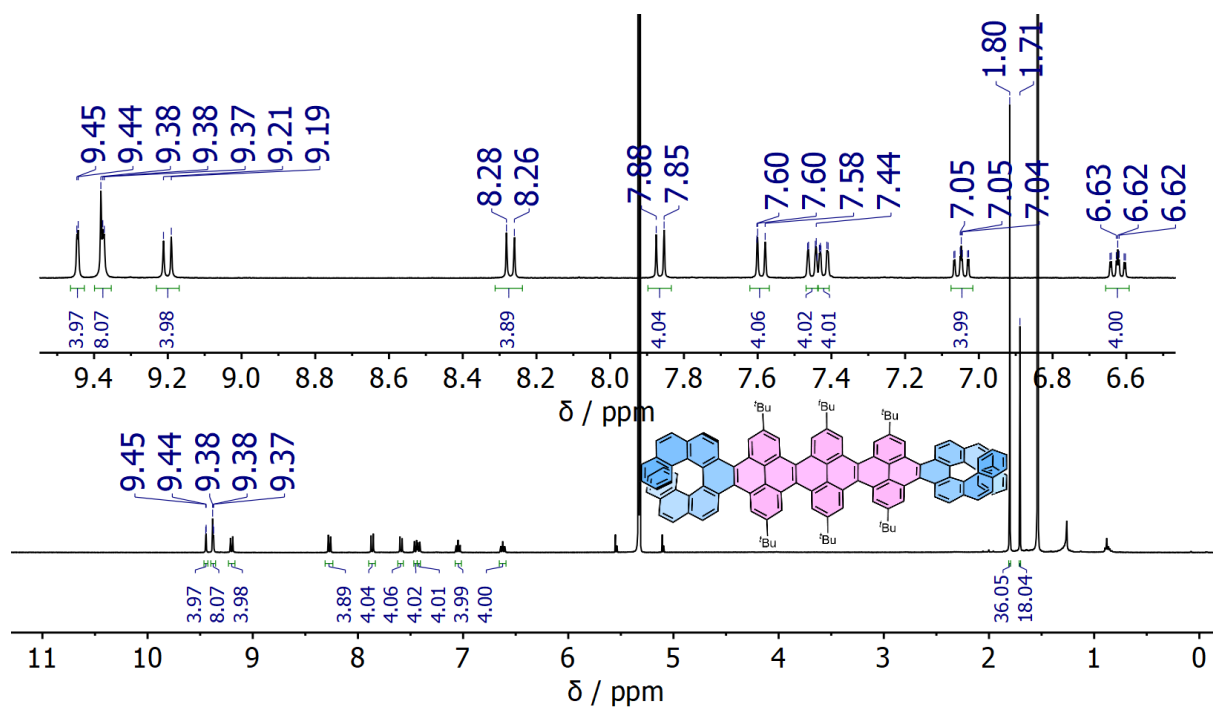
Figure S26. ^{1}H NMR spectrum of (*P, P*)-**2** (400 MHz, CD$_2$Cl$_2$).
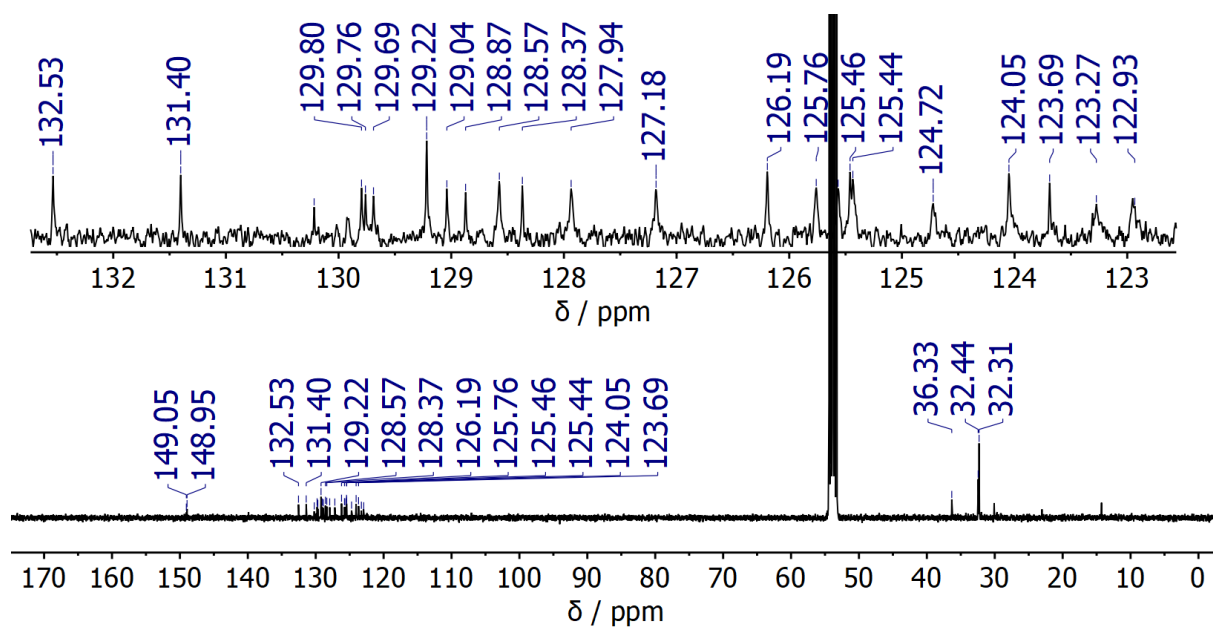
Figure S27. ^{13}C(^{1}H) NMR spectrum of (*P, P*)-**2** (101 MHz, CD$_2$Cl$_2$).
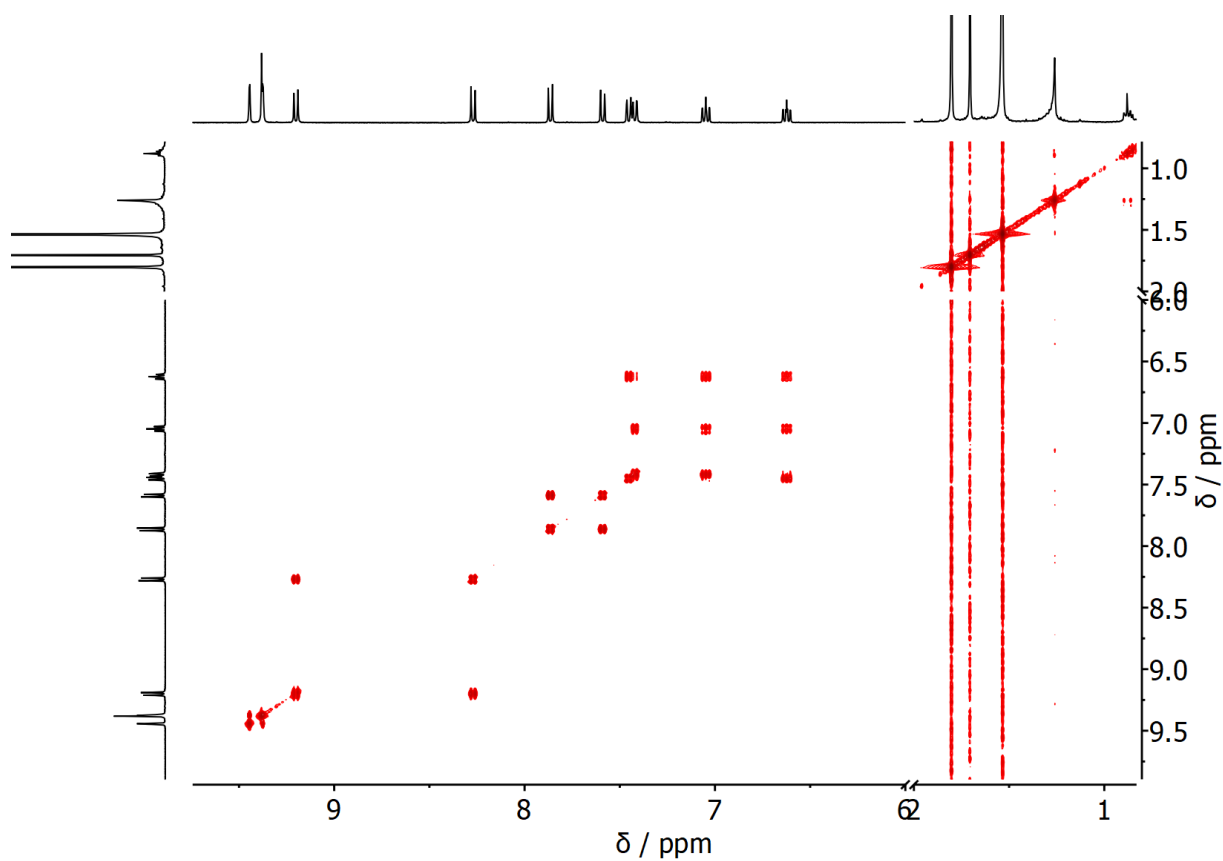
Figure S28. $^1H - {}^1H$ COSY NMR spectrum of (*P, P*)-**2** (400 MHz, CD_2Cl_2).
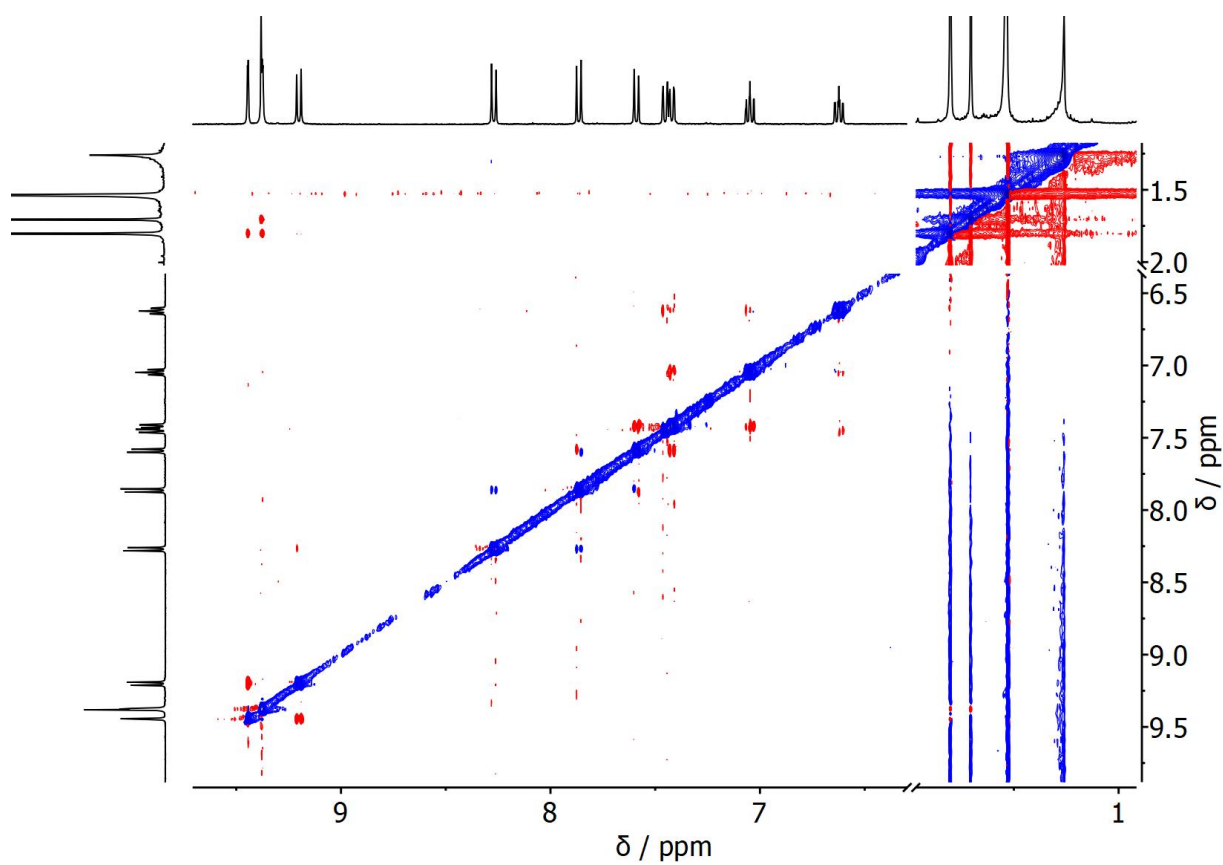
Figure S29. $^1H - {}^1H$ NOESY NMR spectrum of (*P, P*)-**2** (400 MHz, CD_2Cl_2).
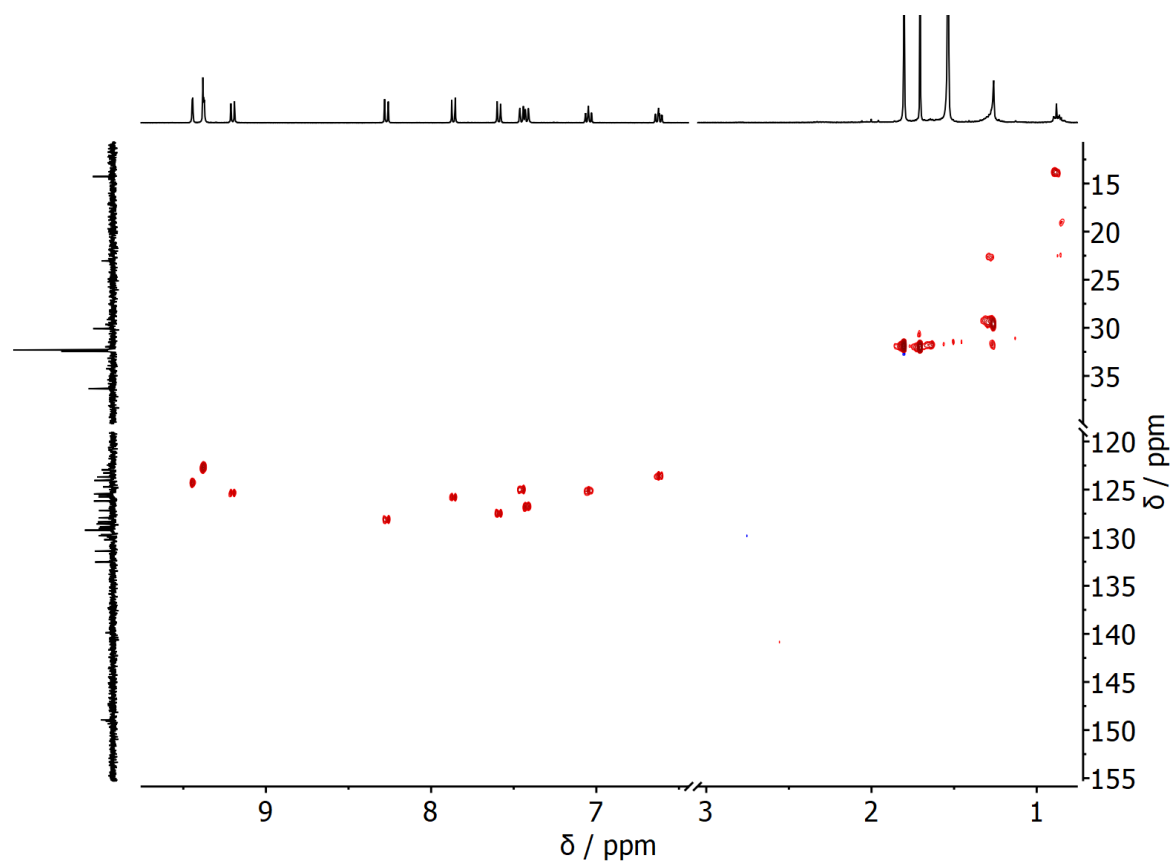
Figure S30. $^1H - ^{13}C$ HSQC NMR spectrum of (*P, P*)-**2** (400 MHz, CD$_2$Cl$_2$).
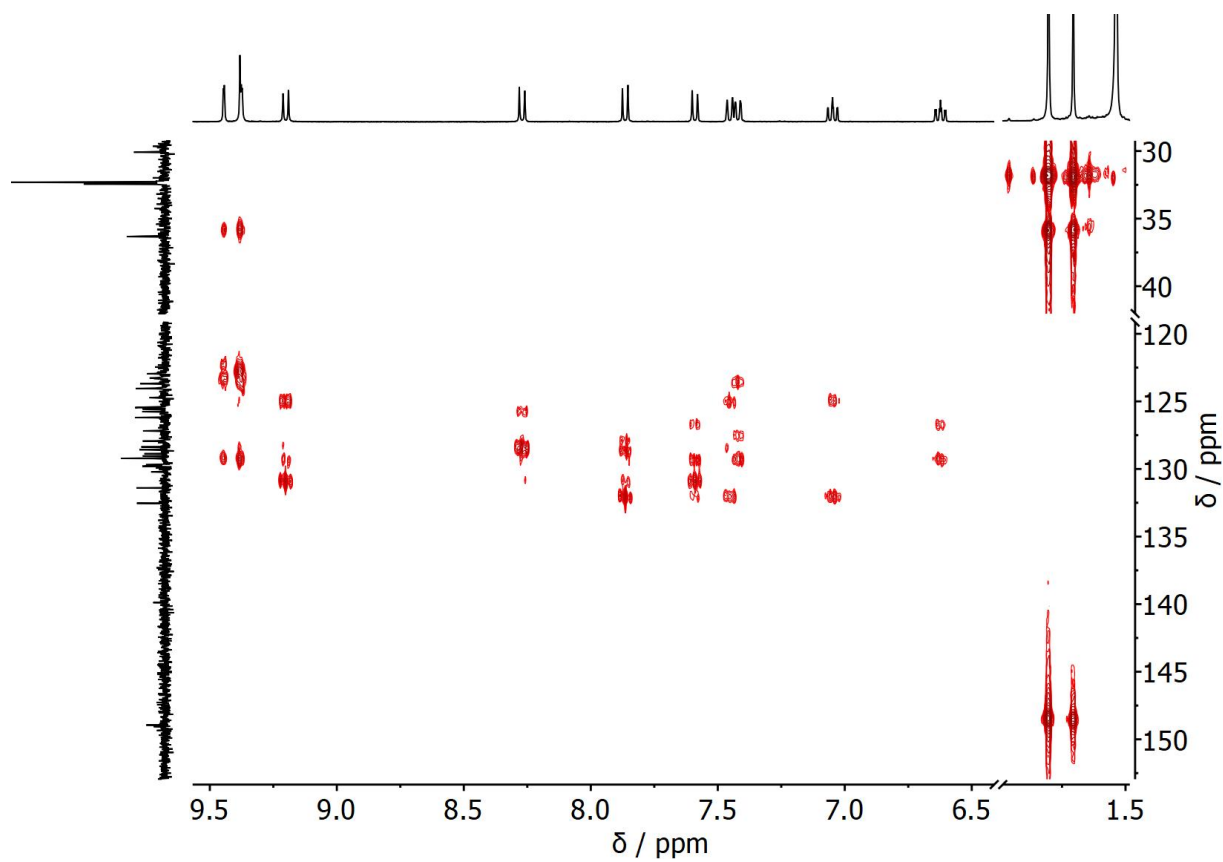
Figure S31. $^1H - ^{13}C$ HMBC NMR spectrum of (*P, P*)-**2** (400 MHz, CD$_2$Cl$_2$).
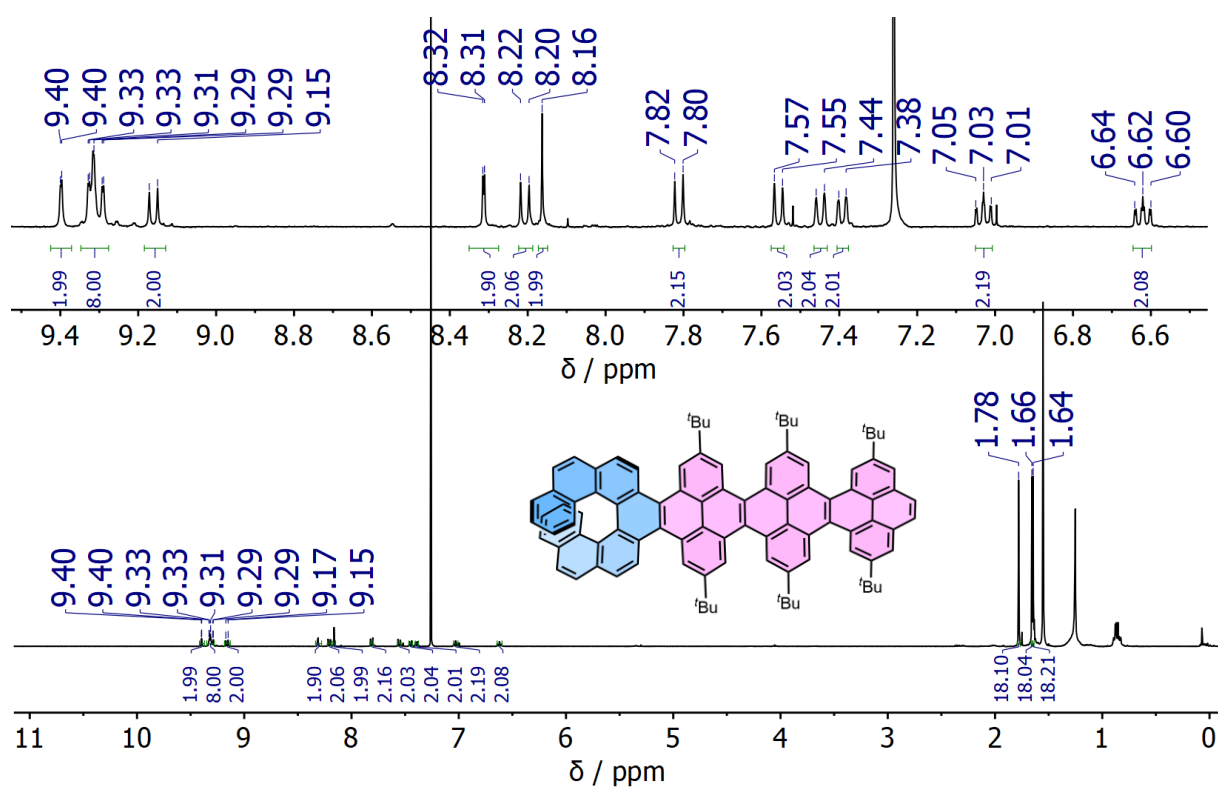
Figure S32. ^{1}H NMR spectrum of (*P*)-**3** (400 MHz, CDCl$_3$).
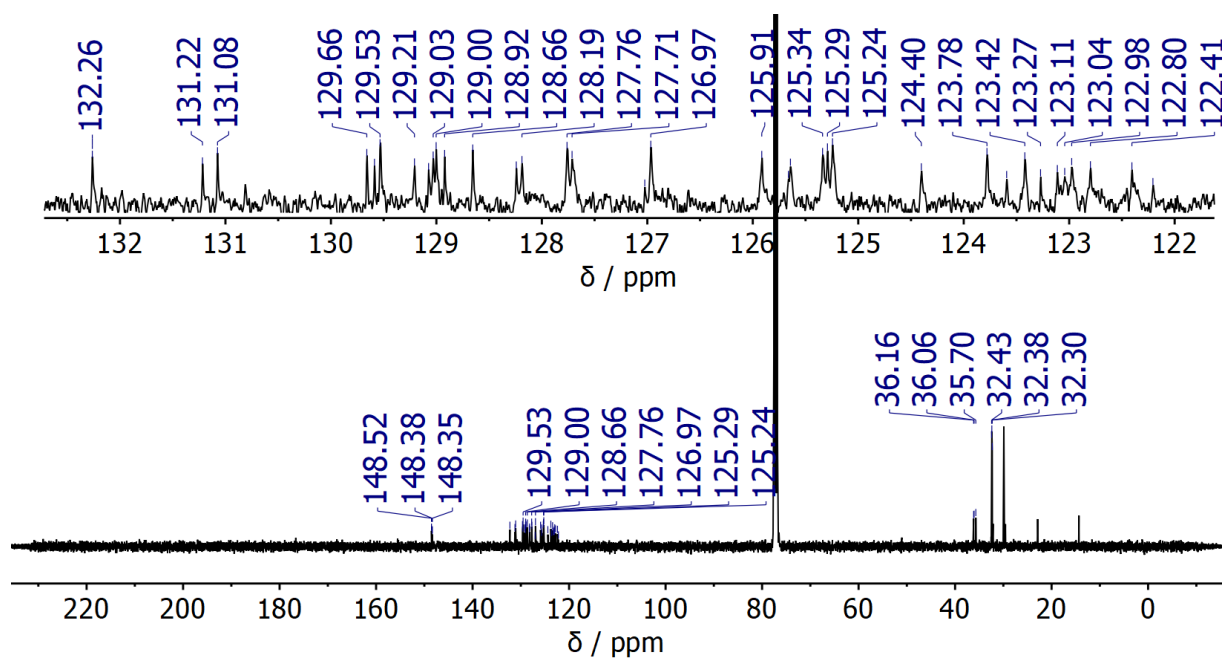
Figure S33. ^{13}C(^{1}H) NMR spectrum of (*P*)-**3** (101 MHz, CDCl$_3$).
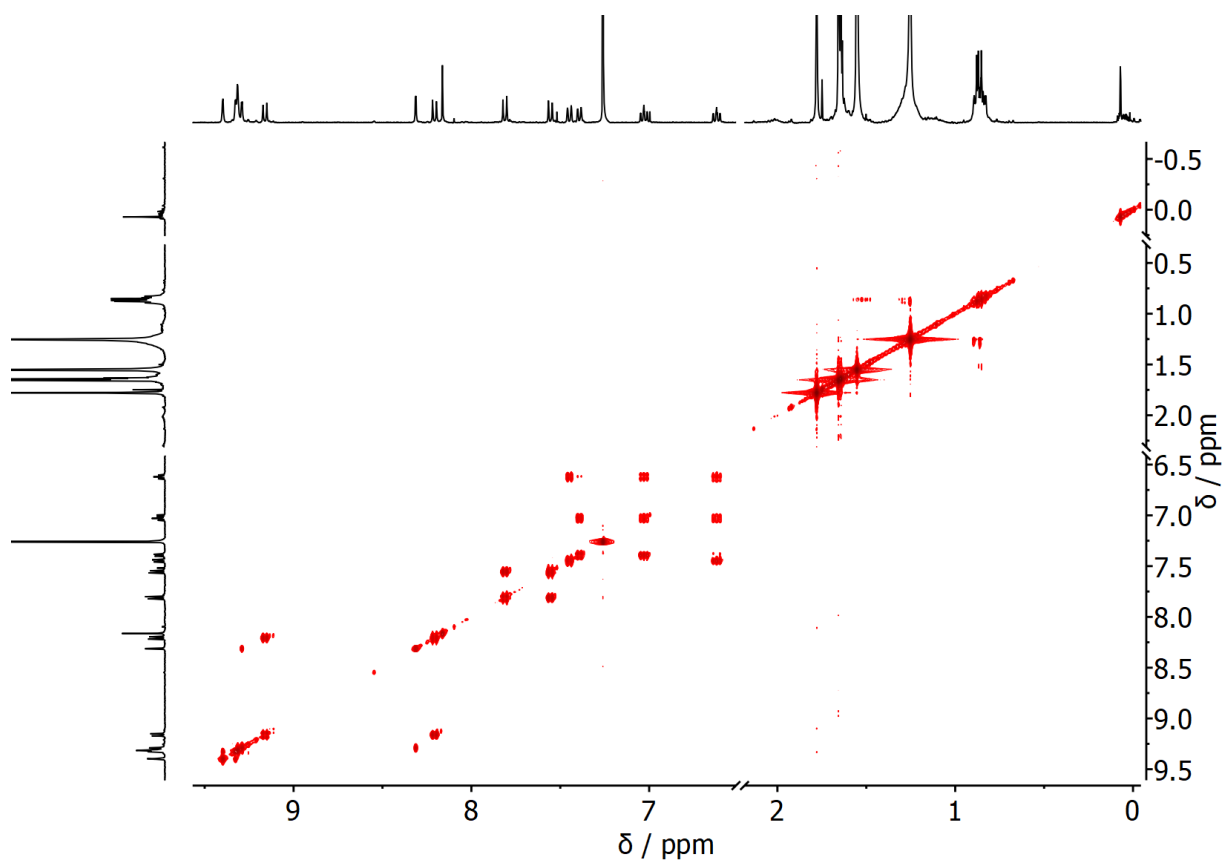
Figure S34. $^{1}H - {}^{1}H$ COSY NMR spectrum of (*P*)-**3** (400 MHz, CDCl$_3$).
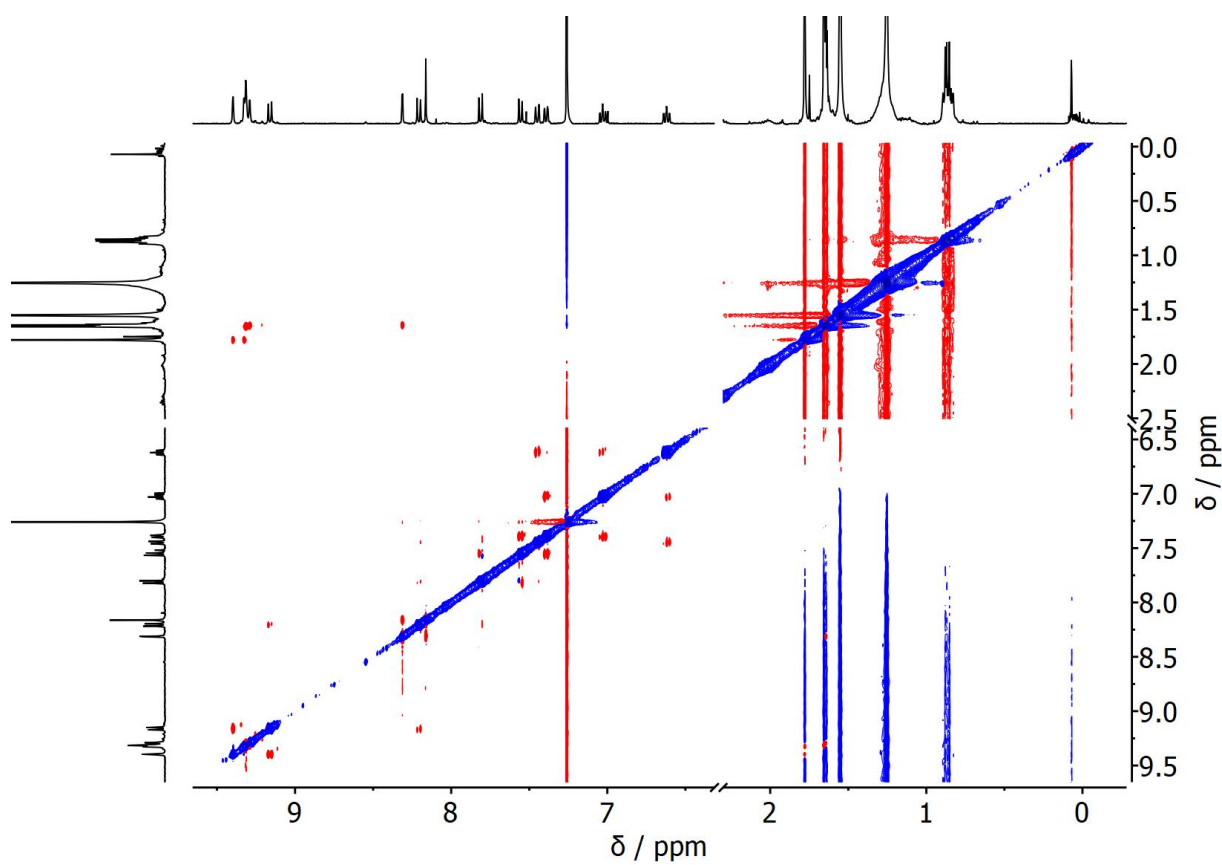
Figure S35. $^{1}H - {}^{1}H$ NOESY NMR spectrum of (*P*)-**3** (400 MHz, CDCl$_3$).

Figure S36. ^{1}H NMR spectrum of (*P*)-**3_Cl** (400 MHz, CDCl$_3$).

Figure S37. ^{13}C(^{1}H) NMR spectrum of (*P*)-**3_Cl** (101 MHz, CDCl$_3$).
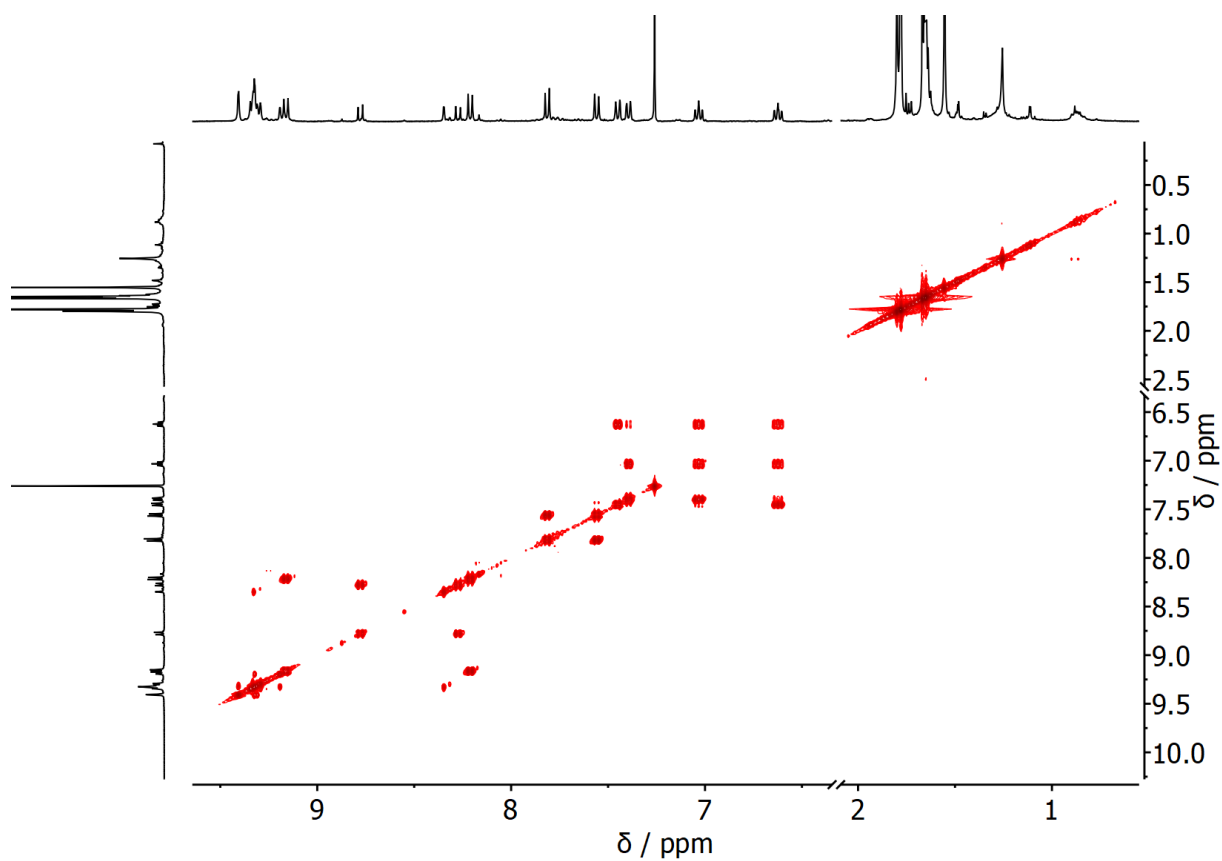
Figure S38. $^1H – ^1H$ COSY NMR spectrum of (*P*)-**3_Cl** (400 MHz, CDCl$_3$).
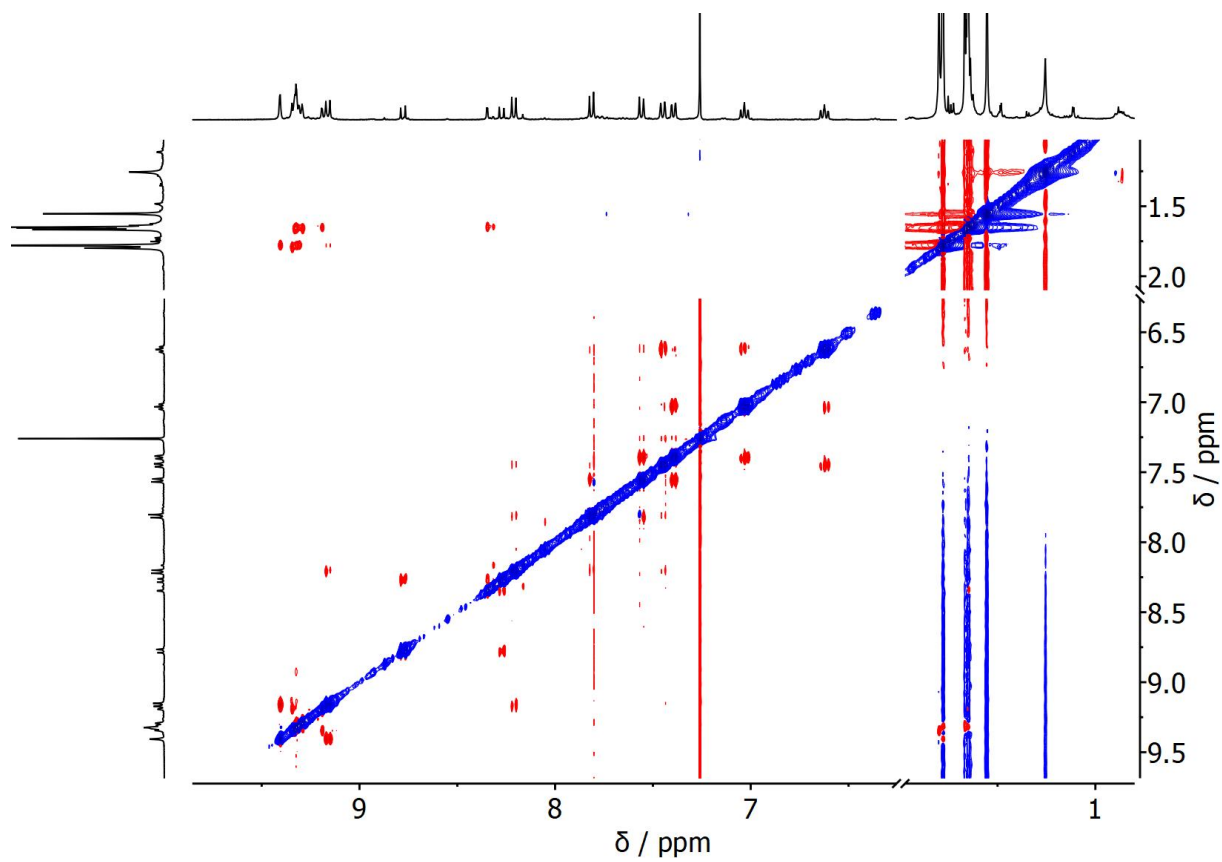
Figure S39. $^1H – ^1H$ NOESY NMR spectrum of (*P*)-**3_Cl** (400 MHz, CDCl$_3$).

S9. High resolution mass spectrometry (HRMS)
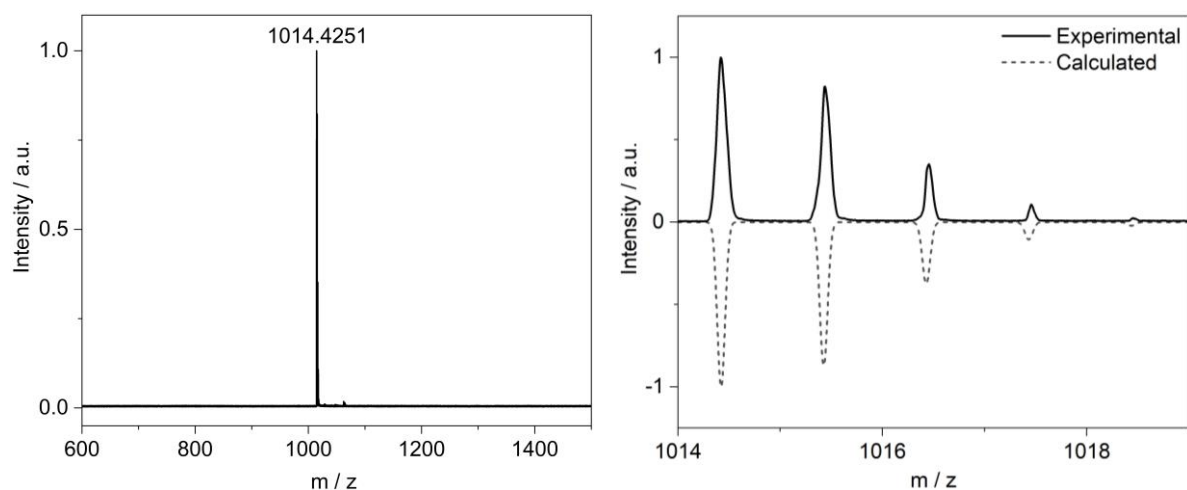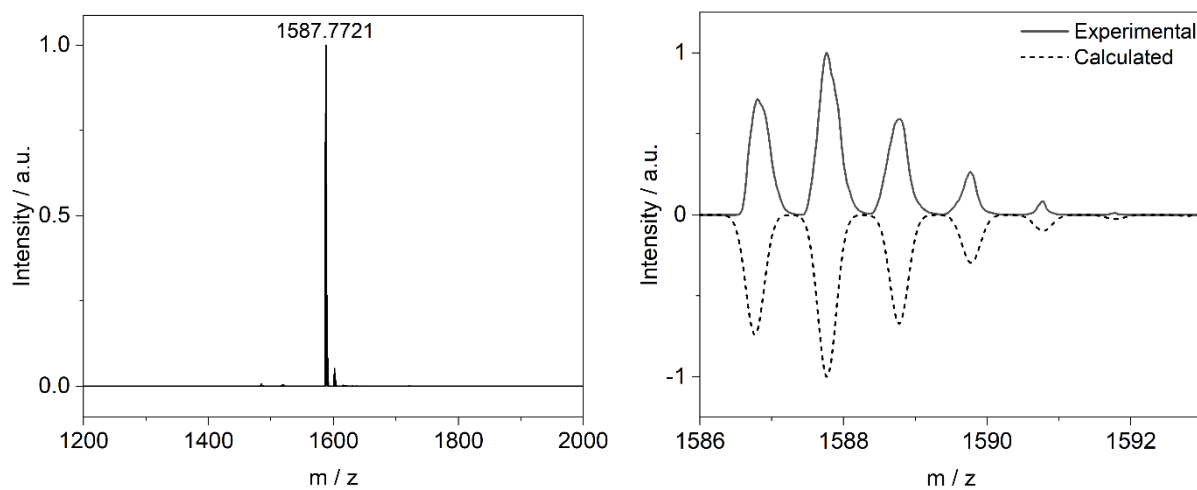

Figure S40. MALDI-TOF HRMS of (*P*, *P*)-**1**.

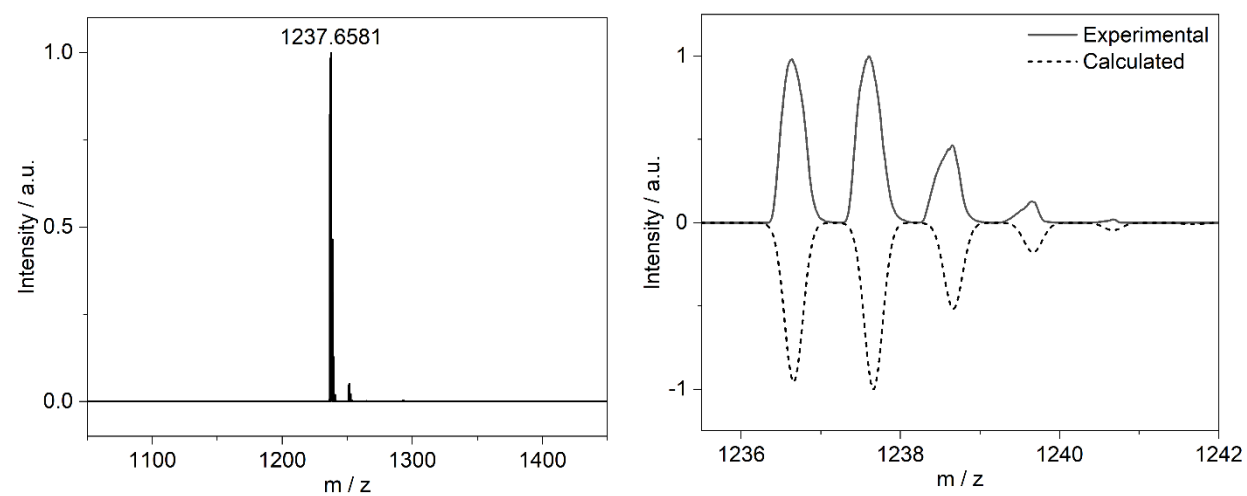

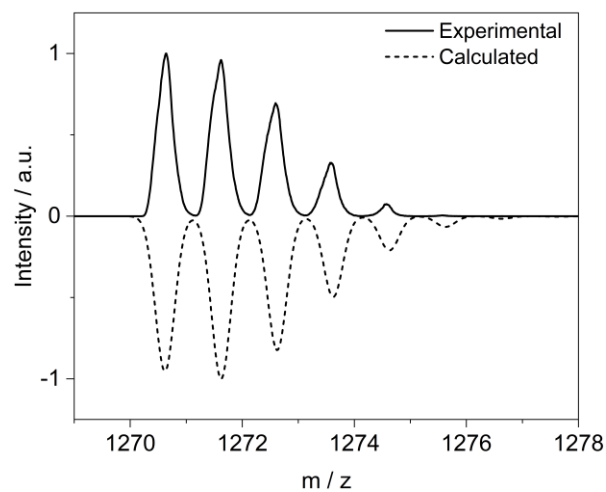**Figure S41.** MALDI-TOF HRMS of (*P*, *P*)-**2**.

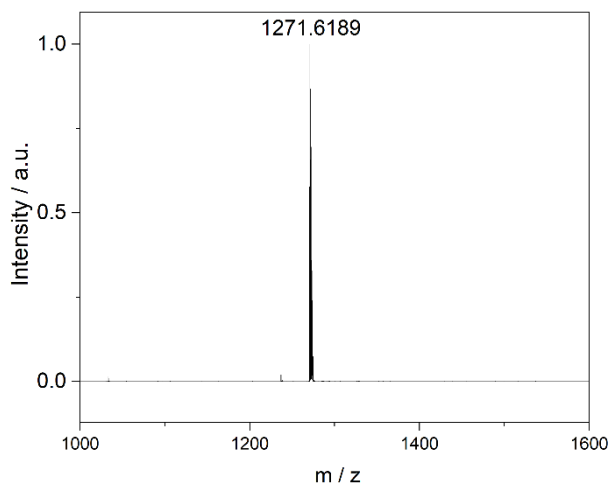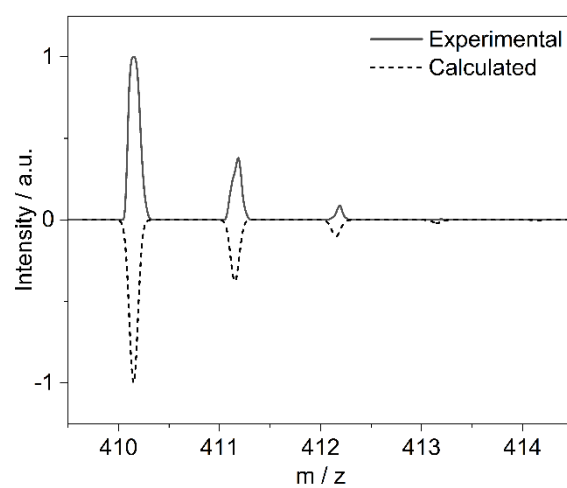**Figure S42.** MALDI-TOF HRMS of (*P*)-**3**.

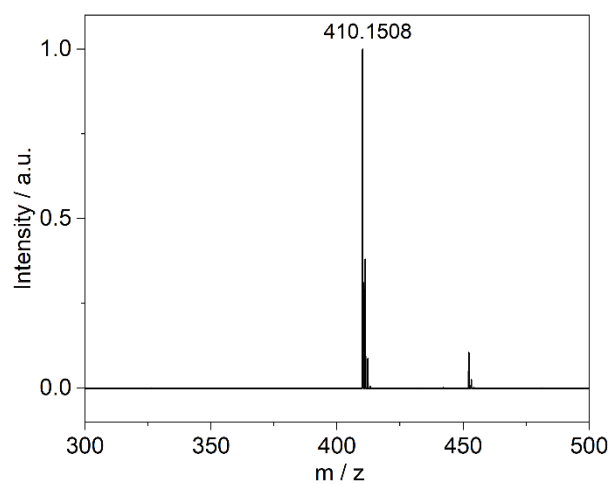**Figure S43.** MALDI-TOF HRMS of (*P*)-**3_Cl**.

Figure S44. MALDI-TOF HRMS of **Sila[7]helicene**.
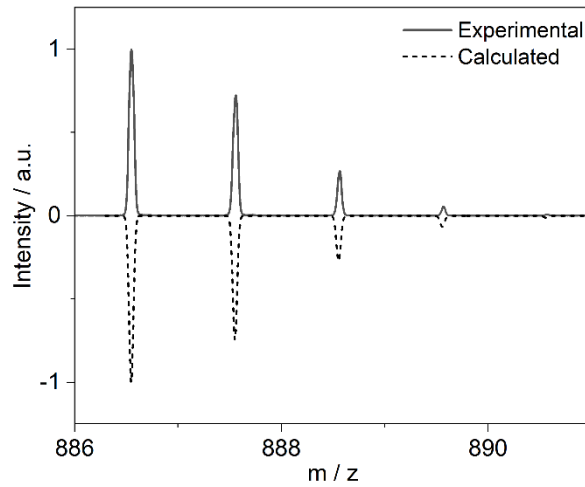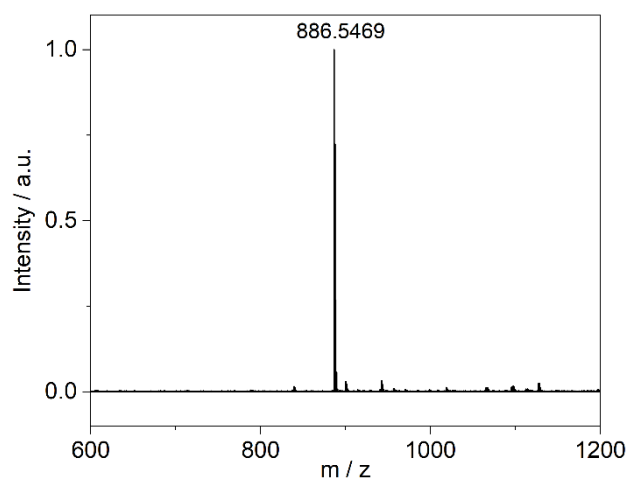

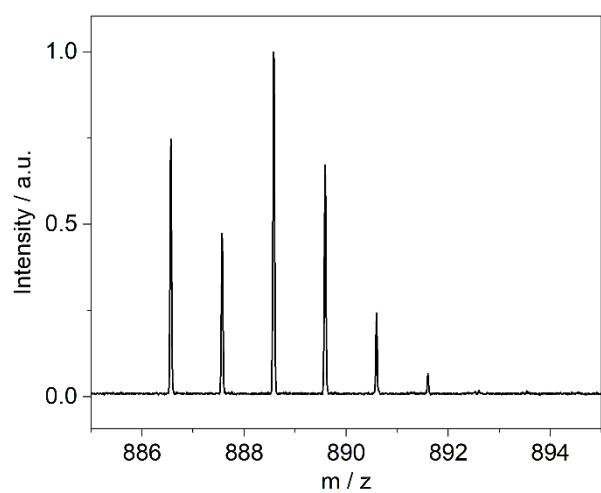**Figure S45.** MALDI-TOF HRMS of **3Py**.

Figure S46. MALDI-TOF MS of crude reaction mixture after Suzuki coupling-C–H activation for preparing **3Py**.

S10. References

[1]   A. K. Swain, K. Radacki, H. Braunschweig, P. Ravat, *J. Org. Chem.* **2022**, *87*, 993-1000.

[2]   Q. Li, J. Li, H. Ren, Z. Gao, D. Liu, *Synth. Commun.* **2011**, *41*, 3325-3333.

[3]   L. Ji, I. Krummenacher, A. Friedrich, A. Lorbach, M. Haehnel, K. Edkins, H. Braunschweig, T. B. Marder, *J. Org. Chem.* **2018**, *83*, 3599-3606.

[4]   Z. Guo, S.-M. Yiu, M. C. W. Chan, *Chem. Eur. J.* **2013**, *19*, 8937-8947.

[5]   K. Ozaki, K. Kawasumi, M. Shibata, H. Ito, K. Itami, *Nat. Commun.* **2015**, *6*, 6251.

[6]   M. Strohalm, D. Kavan, P. Novák, M. Volný, V. Havlíček, *Anal. Chem.* **2010**, *82*, 4648-4651.

[7]   G. Sheldrick, *Acta Crystallogr. A* **2015**, *71*, 3-8.

[8]   G. Sheldrick, *Acta Crystallogr. A* **2008**, *64*, 112-122.

[9]   M. J. Frisch, G. W. Trucks, H. B. Schlegel, G. E. Scuseria, M. A. Robb, J. R. Cheeseman, G. Scalmani, V. Barone, G. A. Petersson, H. Nakatsuji, X. Li, M. Caricato, A. V. Marenich, J. Bloino, B. G. Janesko, R. Gomperts, B. Mennucci, H. P. Hratchian, J. V. Ortiz, A. F. Izmaylov, J. L. Sonnenberg, Williams, F. Ding, F. Lipparini, F. Egidi, J. Goings, B. Peng, A. Petrone, T. Henderson, D. Ranasinghe, V. G. Zakrzewski, J. Gao, N. Rega, G. Zheng, W. Liang, M. Hada, M. Ehara, K. Toyota, R. Fukuda, J. Hasegawa, M. Ishida, T. Nakajima, Y. Honda, O. Kitao, H. Nakai, T. Vreven, K. Throssell, J. A. Montgomery Jr., J. E. Peralta, F. Ogliaro, M. J. Bearpark, J. J. Heyd, E. N. Brothers, K. N. Kudin, V. N. Staroverov, T. A. Keith, R. Kobayashi, J. Normand, K. Raghavachari, A. P. Rendell, J. C. Burant, S. S. Iyengar, J. Tomasi, M. Cossi, J. M. Millam, M. Klene, C. Adamo, R. Cammi, J. W. Ochterski, R. L. Martin, K. Morokuma, O. Farkas, J. B. Foresman, D. J. Fox, Wallingford, CT, **2016**.

[10]   T. Bruhn, A. Schaumloffel, Y. Hemberger, G. Bringmann, *Chirality* **2013**, *25*, 243-249.

[11]   M. D. Hanwell, D. E. Curtis, D. C. Lonie, T. Vandermeersch, E. Zurek, G. R. Hutchison, *J. Cheminformatics* **2012**, *4*, 17.

[12]   H. Oyama, K. Nakano, T. Harada, R. Kuroda, M. Naito, K. Nobusawa, K. Nozaki, *Org. Lett.* **2013**, *15*, 2104-2107.

[13]   F. Liu, X. Shen, Y. Wu, L. Bai, H. Zhao, X. Ba, *Tetrahedron Lett.* **2016**, *57*, 4157–4161.

[14]   A. Sillen, Y. Engelborghs, *Photochem. Photobiol.* **1998**, *67*, 475-486.